On the Global Distribution of Hydrothermal Vent Fields

Edward T. Baker

NOAA/Pacific Marine Environmental Laboratory, Seattle, WA

Christopher R. German

Southampton Oceanography Centre, Southampton, UK

In *Mid-Ocean Ridges: Hydrothermal Interactions Between the Lithosphere and Oceans, Geophysical Monograph Series 148,* C.R. German, J. Lin, and L.M. Parson (eds.), 245–266 (2004)

---

1. INTRODUCTION

After 25 years of seafloor exploration, hydrothermal venting is known to discharge along divergent plate boundaries in every ocean, at all spreading rates, and in a diversity of geological settings. Ever since the discovery of submarine hydrothermal venting, and indeed even before that, prescient researchers have speculated on the global distribution of vent sites and the geologic conditions that control it. Eight years prior to the historic Galápagos discoveries [*Corliss et al.*, 1979], *Boström et al.* [1969] noted that iron- and manganese-rich sediments were preferentially found near "active" oceanic ridges. Moreover, both the extent and Fe+Mn content of these sediments increased with increasing spreading rate, suggesting that volcanism and "mantle outgassing" followed a similar pattern. This observation was the germ of a simple but challenging hypothesis: Hydrothermal activity increases linearly with the magmatic budget. (See *Haymon* [1996] for a succinct history of the development of this hypothesis.) The "magmatic budget" hypothesis was perhaps first articulated by *Francheteau and Ballard* [1983], who envisioned a simple geometry of increased magma supply and hydrothermal activity at segment centers bounded by transform faults.

Testing of this idea was limited for almost a decade by the lack of detailed segment-scale surveys of hydrothermal activity. *Crane et al.* [1985] attempted the first multisegment plume survey, identifying several broad regions of hydrothermally warmed water along the Juan de Fuca Ridge (JDFR). Quantitative support of the link between magma supply and venting was first supplied by *Haymon et al.* [1991], who visually surveyed most of a 2nd-order segment on the East Pacific Rise (EPR), and by *Baker and Hammond* [1992], who used continuous plume mapping to ascertain the distribution of vent sites over an entire 1st-order segment, the JDFR. Accumulation of plume surveys, mostly on fast-spreading ridges, led to the proposal that, on a relative scale, hydrothermal activity increased linearly with spreading rate [*Baker et al.*, 1995, 1996]. *German and Parson* [1998] explored the extension of this relation to the slow-spreading Mid-Atlantic Ridge (MAR). They concluded that while the MAR results generally supported the model, the interplay of magmatic and tectonic processes could create dramatic departures, both positive and negative, from the over-arching linear trend.

In this paper, which includes a wealth of new hydrothermal data gathered since our previous review a decade ago [*Baker et al.*, 1995], we present a comprehensive summary of the distribution of confirmed (from seafloor observations) or inferred (from water column measurements) active hydrothermal sites. We compare distributions on "fast" (rift valley absent) and "slow" (rift valley present) ridges, including a consideration of ultraslow and hotspot-affected ridges, to test the "magmatic budget hypothesis" described above.

While testing of this hypothesis seems straightforward, in fact several factors complicate the task. The most obvious difficulty is that quantitative knowledge of hydrothermal heat or chemical fluxes is rare and imprecise. Thus, we must use qualitative indices for hydrothermal activity, such as plume incidence p_h (the fraction of ridge crest length overlain by a significant hydrothermal plume [*Baker and Hammond*, 1992]), or vent site frequency F_s (sites/100 km of ridge length). Large-scale distributions of plumes are most easily mapped using optical sensors, which are simple, inexpensive, and sensitive. The distributions described here are from light backscattering measurements (or light attenuation measurements transformed to light backscattering), given in terms of

nephelometric turbidity units (NTUs) [*APHA*, 1985], determined from a laboratory calibration using formazine [*Baker et al.*, 2001a]. ΔNTU is the plume optical anomaly in excess of the ΔNTU value of local ambient deep waters.

Another hindrance is the differing temporal scales of magma cycling and hydrothermal venting. Ideally, monitoring of hydrothermal activity at sites spanning the full range of the magmatic budget (or its proxy, spreading rate) at oceanic ridges would test this hypothesis effectively. Unfortunately, the temporal scale required to obtain statistically valid data, perhaps roughly the time required to accrete the full breadth of the neovolcanic zone at each site, is impossibly long. A reasonable alternative is to substitute spatial sampling for temporal sampling. In principle, a survey of multiple tectonic segments of the same spreading rate should provide a statistically significant measure of the hydrothermal activity characteristic of that spreading rate or magmatic budget. The actual ridge length necessary for a reliable survey remains to be established but almost certainly increases as spreading rate decreases. In practice, we consider ~200 km to be a minimum survey size for fast ridges, with longer surveys required for slow ridges.

A third complication is that hydrothermal circulation requires the confluence of a sufficient heat source and adequate permeability. While the availability of magmatic heat along the global ridge system is roughly proportional to the spreading rate, changes in the crustal permeability of the neovolcanic zone at either the local or regional scale are presently unconstrained even in relative terms [e.g., *Fisher*, 1998]. If bulk permeability is a strong function of spreading rate, for example, its effect on the development of hydrothermal circulation could blur the relationship between magma supply and hydrothermal activity [e.g., *German and Parson*, 1998].

The generation of hydrothermal circulation by heat sources other than magma cooling introduces more uncertainty. On slow- and ultraslow-spreading ridges where the basaltic magma flux is weakest, heat from gabbroic intrusions, from cooling of the lithospheric mantle [*Cannat et al.*, 2004; *Bach et al.*, 2002], and from exothermic serpentinization of ultramafic rocks [*Kelley et al.*, 2001; *Schroeder et al.*, 2002; *Lowell and Rona*, 2002] may increase the vent field population. Serpentinization, for example,

may "contaminate" entire segments of slow-spreading ridge with plumes of dissolved products such as CH_4 [*Charlou and Donval*, 1993], complicating the identification of magma-driven hydrothermal venting. Vent fields driven solely by serpentinization reactions will likely not be readily detected using our well established, optically based survey methods, however. Such fluid discharge is rich in dissolved gases but metal-poor, so that the precipitation of Fe-Mn oxyhydroxides following release into the water column is minimal [*Kelley et al.*, 2001].

Finally, the hydrothermal data set to be considered must be representative of activity on ridges of all spreading rates. While it may be premature to characterize the available data as truly globally representative, we now have at least preliminary hydrothermal surveys from ridge sections across the entire spectrum of spreading rates.

2. THE GLOBAL VENT FIELD DISTRIBUTION

2.1 Vent Field Locations

Large-scale, systematic searches for undiscovered vent sites have been organized with increasing frequency since the early 1990s [*Baker et al.*, 1995; *German et al.*, 1995] and now span the global range of spreading rates. The practical difficulty of comprehensively imaging vent fields means that the most efficient searches rely on inferring their presence from water column observations, a technique that carries varying levels of uncertainty. The enrichment of hydrothermal fluids in several key chemical tracers (e.g., Mn, Fe, CH_4, H_2, ^3He) relative to deep ocean waters offers an unambiguous method for detecting hydrothermal discharge even kilometers away from seafloor vent sites. As early as 1985 it became clear that optical properties (light transmission or backscattering) could be effective proxies for chemical anomalies in plumes [*Baker et al.*, 1985; *Klinkhammer et al.*, 1986; *Nelsen et al.*, 1986/87]. This conformity validates many recent plume surveys, which are often ancillary projects combined with geophysical or rock-sampling operations that do not include plume water sampling. These projects almost uniformly measure only optical properties of the water column, because these data are sensitive, economical, simple to collect, and almost invariably provide a reliable indicator of underlying hydrothermal activity. Interpretative difficulties can arise,

however, especially on slow-spreading ridges, which generally exhibit greater relief and thicker sediment accumulation than fast ridges. Under these conditions, the potential for a false positive (as from sediment resuspension around complex bathymetry) is increased.

A review of the literature, existing vent-field databases, and unpublished sources enumerates ~280 sites of active hydrothermal venting on spreading ridges (including back-arc spreading centers), volcanic arcs, and intraplate volcanoes (Figure 1a). Details of each site including (where available) location, water depth, ridge spreading rate at the site location, and literature reference are available on the InterRIDGE web site (http://www.interridge.org). Some 145 of these sites have been confirmed by visual observation or imagery, while another ~130 are inferred solely from water-column observations. Confirmed vent sites range from isolated patches of low-temperature diffuse flow to enormous sulfide constructs hosting multiple high-temperature chimneys. Precise enumeration of these vent sites is necessarily subjective in the absence of any clear definition of a "vent field." Discharge along fast- and intermediate-rate ridges can be common for kilometers along axis, and investigators sometimes give unique names to vent sites only 10s or 100s of meters apart. In this paper, we have aggregated some of these crowded areas into single sites. Vent sites inferred from plume observations range from plumes unequivocally identified as hydrothermal from a combination of optical, hydrographic, and diagnostic chemical measurements, to minor optical anomalies that may ultimately prove unrelated to hydrothermal discharge. As with seafloor enumerations, a single plume observation reported here may arise from a single isolated source or from multiple but closely spaced vent fields extending for several kilometers along axis.

Despite these caveats, the data distribution along ridges shows several robust trends. Over half (118) of our 222 known or inferred ridge vent sites occur on the heavily surveyed eastern Pacific ridges. Only one-fifth as many (24) have been discovered on the MAR, and all confirmed sites there fall within a narrow latitudinal band between 15° and 38°N, reflecting historic funding/research priorities within the international community. In the southern hemisphere, only two confirmed sites, both near the Rodriguez Triple Junction in the Central Indian Ocean, have been observed along a continuous ~30,000 km

chain of ridge crest that includes the southern MAR, all of the SW, Central, and SE Indian Ocean ridges, and the Pacific Antarctic Ridge/East Pacific Rise south of 38°S. Plume surveys, however, have so far identified 25 targets along that same stretch of ridge, almost entirely on Indian Ocean ridges. While the focus of this paper is on vent sites along divergent plate boundaries, we note that intensive surveying efforts on volcanic arcs, especially since 1999, have found 58 confirmed or inferred sites, 20% of the global total [*Ishibashi and Urabe*, 1995; *de Ronde et al.*, 2003; *Embley et al.*, 2004]. In general, these sites remain understudied relative to ridge sites.

The usefulness of this distribution depends largely on its accuracy and completeness. Based on the spatial density of acquired data, we identify three types of surveyed areas along the global ridge system (Figure 1b). The most reliable statistics come from densely surveyed areas, where detailed water column and/or seafloor investigations provide excellent control on where vent fields are, and, equally importantly, are not. Human or photographic imaging of the seafloor provides the most meticulous surveying, but is an exceedingly inefficient mode of data-collection when compared to plume surveys and presently accounts for only a small fraction of mapped ridges. In most densely surveyed areas, hydrothermal plumes have been mapped either continuously (e.g., by a towed instrument package) or by closely spaced vertical profiles. These areas cover a total of ~4900 km of ridge axis and are most common along the eastern Pacific ridges, but also include the Reykjanes Ridge south of Iceland, areas around the Rodriguez Triple Junction in the Indian Ocean, the western Gakkel Ridge, and other scattered sections (Figure 1b). Moderately surveyed areas have undergone systematic searches for hydrothermal activity, but the spatial density of the data is lower than in densely surveyed areas and, thus, is not comprehensive. Within this category, therefore, it is quite probable that more active vent sites may exist than those that have actually been discovered to date. These moderately surveyed areas are most common on slow- and intermediate-rate spreading ridges and total ~4900 km (Figure 1b). Sparsely surveyed areas have been sampled in sufficient detail to locate the presence of confirmed and/or likely vent sites, but considerable uncertainty remains about the full extent of hydrothermal activity in those areas. This category totals ~3500 km of ridges and includes the Chile Rise and

several large sections in the Atlantic Ocean (Figure 1b). Together, these three categories of surveyed areas still total only ~13,000 km of ridge length, or ~20% of the ~67,000 km [*Bird*, 2003] of global ridges (including ~6500 km in back-arc basins). Other ridge vent and plume sites fall outside these areas, of course, because they were discovered serendipitously, rather than as part of any systematic, large-scale hydrothermal survey.

2.2 Vent Field Statistics

If we restrict our attention to vent fields on ridges (oceanic and back arc), a histogram of the water depths at which confirmed and inferred vent fields occur describes a distribution range from 200 to 4300 m, with highest frequencies at depths between 2200 and 2800 m (Figure 2a). Depths of those sites inferred from plume surveys are strongly skewed toward deeper waters, reflecting a concentration of recent plume surveys along ultraslow ridges [*German et al.*, 1998a; *Bach et al.*, 2002; *Edmonds et al.*, 2003]. Only one site on an ultraslow ridge has actually been observed, at a confirmed depth of 4100 m on the Gakkel Ridge [*Edmonds et al.*, 2003]. The depth reported for each inferred site in Figure 2a is the depth of the shallowest feature on the underlying rift-valley floor close to the location of the plume observation. Plotting frequency of vent sites against spreading rate results in a complex histogram with peaks at slow-, intermediate-, fast-, and superfast-spreading rates (Figure 2b). From this figure it is clear that the ratio of confirmed to inferred sites increases from the slowest to the fastest spreading rates, a testimony to the historical pattern of seafloor hydrothermal exploration. This distribution is also quite different from that for the cumulative length of ridge crests themselves vs. spreading rate (using data from *DeMets et al.* [1990] and *Bird* [2003]), which shows a general decline in ridge length at increasing spreading rates (Figure 2c). For example, ridges spreading faster than 120 mm/yr comprise only 9% of the total length of the global ridge system, but account for 27% (60) of the presently recognized ridge vent field total, a sum consistent with the 26% of total crustal volume generated each year along these ridges. Note, however, that fast-spreading ridges are currently oversampled compared to the rest of the ridge system. About 30% of ridges spreading faster than 100 mm/yr have

been surveyed at least "densely" or "moderately," compared to only 12% of the ridges spreading slower than 80 mm/yr (Figure 2c).

3. "FAST" RIDGES

"Fast" ridges are defined here as those having a narrow and shallow (relief on the order of 100 m or less) axial valley. This category typically ranges from intermediate (55–80 mm/yr) to superfast (>140 mm/yr) spreading rates. We use this definition because it describes ridge sections where virtually all detectable hydrothermal discharge is concentrated in or near a narrow neovolcanic zone, and where hydrothermal plumes can be readily dispersed off axis by local currents. These qualities allow efficient and credible surveying for hydrothermal plumes (and their seafloor sources), and make it likely that the plume distribution will be a reliable indicator of the location and extent of the seafloor sources (i.e., plumes are unlikely to be transported long distances along axis).

Among the best places to demonstrate the capability of optical plume transects to denote the spatial density of seafloor vent fields is the EPR between 13.5° and 18.67°S (Figure 3), the focus of several submersible, remotely or autonomously operated vehicle, and plume survey campaigns that have systematically surveyed for vent sites [*Renard et al.*, 1985; *Urabe et al.*, 1995; *Auzende et al.*, 1996; *Haymon et al.*, 1997; *Lupton et al.*, 1997; *Embley et al.*, 1998; *Von Damm et al.*, 1999; *Lupton et al.*, 1999; *Wright et al.*, 2002]. A continuous plume transect here using an optical light backscattering sensor on a conductivity-temperature-depth-optical (CTDO) package in the "tow-yo" mode [*Baker et al.*, 1995] found p_h = 0.60 [*Baker and Urabe*, 1996]. Comparing the ΔNTU distribution with discrete particulate (Fe) and dissolved (CH_4) chemical tracers confirms that the optical signal reliably described the distribution of all significant hydrothermal plumes on this section of the EPR (Figure 3). How well does the plume data reflect the seafloor sources? Water column data identify approximately six discrete plume maxima between 14° and 17°S, plus a continuous and variable plume from 17.33° to 18.67°S (Figure 3a). While submersible and remotely/autonomously operated vehicle expeditions have transited only ~10% of this ridge section, these expeditions have nevertheless located

active vent fields under five of the discrete plumes and throughout the 17.33°–18.67°S area. This substantial agreement between the location of the mapped vent fields and hydrothermal plumes implies that no significant vent fields went undetected by the plume surveys, though future volcanic activity will certainly create new fields even as some old fields grow extinct.

In addition to the EPR section described above, continuous plume data have been acquired along three other multisegment sections of fast-spreading ridge: the Juan de Fuca/Explorer Ridge [*Baker and Hammond*, 1992; E.T. Baker, unpublished data], the EPR 8.67°–11.83°N [*Baker et al.*, 1994], and the EPR 27.5°–32.3°S [*Baker et al.*, 2002] (Table 1). To compare the plume distributions along all four ridge sections, we compile transects of vertically integrated ΔNTU (ΣΔNTU). ΣΔNTU is calculated by gridding the two-dimensional ΔNTU transects (e.g., Figure 3a) at cell sizes of x = 0.03° of latitude (~3 km), y = 25 m, then vertically summing ΔNTU in each x interval from the seafloor to plume top. The ΣΔNTU plots (Figure 4) illustrate that as spreading rate increases not only does p_h increase, but so does the along-axis extent of the largest plume features. On superfast ridge sections, vent sources can be so extensive that plumes are continuous for upwards of 100 km along axis.

Two other fast ridge sections without continuous plume data still meet the criteria of having multisegment extent and a sufficiently high density of individual plume profile data to reliably calculate p_h: the EPR 15.33°–18.5°N [*Baker et al.*, 2001b] and the South East Indian Ridge (SEIR) 77°–88°E [*Scheirer et al.*, 1998]. For these types of data sets, *Scheirer et al.* [1998] argued that sufficiently closely spaced vertical profiles represent a statistically valid subsampling of the continuous plume distribution, such that the p_h value is equivalent to the percentage of vertical profiles that detect a hydrothermal plume. The SEIR section is unusual in that about one third of the ridge length studied bisects the Amsterdam-St. Paul Plateau, a hotspot location with a crustal thickness of ~10 km [*Scheirer et al.*, 2000]. Hydrothermal plumes there were mapped using 81 vertical light-scattering/temperature profiles collected at an average spacing of 18 km with Miniature Autonomous Plume Recorders (MAPRs [*Baker and Milburn*, 1997]) attached to dredges and rock cores. *Scheirer et al.* [1998] recognized plumes on 11 of those 81 profiles

(including one in the caldera of an off-axis volcano), yielding a maximum p_h of 0.14 for the entire area. For reasons we discuss below, hydrothermal circulation along ridge sections that overlie mantle hotspots may be markedly affected by their characteristic thickened crust and higher mantle temperatures [e.g., *Chen*, 2003]. We have partitioned our data for the SEIR survey, therefore, into those ridge sections intersecting the hotspot influence and those adjacent to it [*Scheirer et al.*, 2000]. Outside of the hotspot-influenced region, 36 profiles along 1050 km of ridge axis produced 6 plume sites, for a $p_h = 0.17$.

The data summarized above span spreading rates from intermediate to superfast, and if the long-term magma budget is the primary control on hydrothermal activity we should expect a robust correlation between the magma delivery rate, V_m, and both p_h and F_s. We estimate V_m from

$$V_m = T_c u_s$$

where T_c is the nominal crustal thickness of 6.3 ± 0.9 km for ridges with a full spreading rate (u_s) > 20 mm/yr [*White et al.*, 1992, 2001] (Table 1). Plotting F_s (Table 1) against V_m yields a scattered relationship that reflects not only the observed distribution of hydrothermal activity, but also the current intensity of seafloor exploration effort and the uncertainty in enumerating vent fields on fast-spreading ridges (Figure 5a). The JDFR has been explored for over 20 years, while a submersible has yet to visit the EPR 15.33°–18.5°N or SEIR areas. We can improve the statistics dramatically, however, by binning these six sections according to superfast, fast, and intermediate spreading rates so that each data point represents at least 500 km of ridge length (Figure 5c). The more robust relationship obtained by plotting p_h against V_m demonstrates the integrating value of multisegment plume surveys in determining relative hydrothermal activity (Figure 5b). The evidence is compelling in either case: multisegment hydrothermal activity along "fast" ridges is primarily controlled by the magmatic budget.

4. "SLOW" RIDGES

We define "slow" ridges as those with deep, spacious, and generally enclosed rift valleys, commonly with several hundreds of meters of relief, typically spreading at rates between 20 and 55 mm/yr (we discuss ultraslow-spreading ridges separately, below). These characteristics create a challenging environment for identifying and locating vent sites. The frequent absence of a well-defined neovolcanic zone and the presence of deep and enduring faults that facilitate the discharge of hydrothermal circulation over a broad expanse of seafloor make survey strategies far more complex than on fast ridges. Even when plumes are detected, their source is typically not obvious because the rift valley relief may trap and disperse a plume throughout much or all of an individual tectonic segment [e.g., *German et al.*, 1998b; *Bougault et al.*, 1998].

The first systematic investigations for submarine hydrothermal activity on any slow-spreading ridge were conducted on the northern MAR (11°–26°N) in the 1980s [*Klinkhammer et al.*, 1985; *Bougault et al.*, 1990; *Charlou and Donval*, 1993]. Those preliminary investigations relied upon vertical casts within individual segments of the MAR rift valley to detect midwater chemical anomalies (e.g., total dissolvable (TD)Mn, dissolved CH_4) indicative of hydrothermal discharge from the seafloor. This "point-sampling" approach found midwater TDMn anomalies in nine segments of the MAR between 11° and 26°N [*Klinkhammer et al.*, 1985], and midwater CH_4 enrichments in 14 segments within the same region [*Charlou and Donval*, 1993]. Subsequent detailed studies within this region discovered major vent fields such as TAG [*Rona et al.*, 1986], Snake Pit [*ODP Leg 106 Scientific Party*, 1986], and Logatchev [*Krasnov et al.*, 1995]. Other "point-sampling" surveys have identified more than 10 additional sites between 40°N and 8°S where chemical and/or optical anomalies indicate the presence of hydrothermal plumes but are insufficient to locate the precise source of venting (Figure 6) [e.g. *Charlou et al.*, 1991; *Aballéa et al.*, 1998; *Chin et al.*, 1998; *German et al.*, 2002].

Unlike on fast ridges, plume surveys on slow ridges have been either too imprecise or too short to yield reliable estimates of p_h. (Note that we are here adopting a more rigorous interpretation than we have used earlier [e.g., *Baker et al.*, 1995, 1996], where MAR p_h values were estimated from vent site frequency.) Lengthy surveys have been conducted from 27° to 30°N [*Murton et al.*, 1994] and 35.7° to 38°N [*German et al.*,

1996a], but in both cases using only a single transmissometer mounted on the Towed Ocean Bottom Instrument (TOBI) sidescan vehicle towed 150–500 m above bottom. Plumes have been mapped in detail along the Broken Spur [*German et al.*, 1999] and Rainbow [*German et al.*, 1996b] segments, but both surveys extended for no more than ~50 km along axis.

While we have insufficient data to reliably determine p_h, we can calculate minimum estimates of F_s for the two MAR sections mentioned above (we discuss the Reykjanes Ridge below). From 27° to 30°N only the Broken Spur vent field is known [*German et al.*, 1999], yielding a minimum F_s of 0.30. Multiple surveys in the 35.7°–38°N section have located at least three high-temperature hydrothermal sites (Menez Gwen [*Fouquet et al.*, 1995], Lucky Strike [*Langmuir et al.*, 1993], and Rainbow [*German et al.*, 1996b; *Fouquet et al.*, 1997]), and two low-temperature sites (Mt. Saldanha [*Barriga et al.*, 1998] and Menez Hom [*Fouquet et al.* 2002]). Five other sites have been inferred from water column profiles only (in the South Lucky Strike, north FAMOUS, AMAR, and South AMAR segment sections [*German et al.*, 1996a; *Chin et al.*, 1998]), but these inferences are based on very limited data. F_s values thus range from 2.2 to 4.3. Merging the 27°–30°N and 35.7°–38°N sections results in an F_s of 1.5 over 560 km of ridge crest (Figure 5a). *German and Parson* [1998] undertook a similar analysis over a more extended ridge length with consequently weaker data constraints. They found a vent field spacing of ~130 km from 11°–30°N (F_s = 0.77), shrinking to every 30 km from 35.7°–38°N (F_s = 3.3). Merging these two estimates yields a mean F_s of 1.3, consistent with our analysis of the combined 27°–30° and 35.7°–38°N regions (F_s = 1.5).

These MAR surveys have documented that hydrothermal activity on slow ridges can be influenced not only by the magmatic budget but by local tectonic processes as well. Sites closely associated with axial neovolcanic activity include Menez Gwen, Lucky Strike, Broken Spur, and Snake Pit (Figure 6). Other sites occur not at magma-rich segment centers but at the confluence of cross-cutting fault populations on segment walls (TAG, Logatchev), or in segment-end nontransform offsets (NTOs) (Rainbow, Mt. Saldanha, Menez Hom, and other unnamed sites). The apparent increased incidence of

venting between 35.7°N and 38°N, compared to the Kane-Atlantis (24°–30°N) section (Figure 6), led to a "tectonic control of venting" hypothesis [*German et al.*, 1996a; *German and Parson*, 1998; *Gràcia et al.*, 2000; *Parson et al.*, 2000]. This hypothesis argues that obliquity of the axial strike in the 35.7°–38°N area results in a greater number of short 2nd-order ridge segments and larger NTOs than found farther south. Crustal permeability is enhanced within the NTOs by deeply penetrating and long-lived faults, allowing seawater to mine heat not only from crustal magma but also from gabbroic intrusions or cooling in the lithospheric mantle [*Cannat et al.*, 2004], and from exothermic serpentinization [*Schroeder et al.* 2002; *Lowell and Rona*, 2002]. Recent drilling at 14°–16°N on the MAR, for example, suggests the crust there may be 25% gabbroic [*Kelemen*, 2003], and crystallization of such rocks at depths to 20 km might provide a deep heat source in basalt-poor ridge segments. The Rainbow vent field perhaps best exemplifies this hypothesis: it is situated at the intersection of the ridge-axis and an NTO, at 36.25°N on the MAR, and vents 362°C "black smoker" fluids with distinctive chemical compositions indicative of "contamination" by the products of serpentinization reactions at depth [*Holm and Charlou*, 2001; *Douville et al.*, 2002; *Charlou et al.*, 2002]. Sites such as the Lost City Field at 30°N [*Kelley et al.*, 2001] and Mt. Saldanha at 36.51° [*Barriga et al.*, 1998] appear to be driven almost purely by serpentinization. Their low temperature (<100°C) and metal-poor (and thus optically invisible) discharge makes systematic searches for additional sites of this type, which may be pervasive along all slow-spreading ridges, a demanding future challenge.

If processes other than variability in the magmatic budget play a significant role in controlling the distribution of hydrothermal activity on slow ridges, we might expect the MAR not to agree with the trend of fast ridges on a plot of F_s vs. V_m. While F_s for the 27°–30°N and 35.7°–38°N MAR sections are quite different, their weighted mean value closely follows the fast ridge trend (Figure 5a). Thus, the available data are insufficient to reject the magmatic budget hypothesis for slow ridges. While significant departures from the linear trend are clearly observed along individual short segments, what is indisputable is that more extensive and systematic surveys along slow-spreading (20–55 mm/yr) ridges are required to fully test the hypothesis. Currently, the database for these ridges is

smaller than for any other ridge class, even though they constitute ~40% of the global ridge total (Figure 5c).

5. ULTRASLOW RIDGES

Ultraslow ridges are of particular interest because both geochemical and geophysical inferences indicate that the amount of melt generated in the mantle beneath ridges decreases abruptly as spreading rates drop below ~20 mm/yr [*Reid and Jackson*, 1981; *White et al.*, 2001]. Magmatism becomes discontinuous and mantle peridotite is emplaced directly to the seafloor over broad areas, creating a class of ridge fundamentally different from all faster-spreading ridges [*Dick et al.*, 2003]. If the spatial density of hydrothermal circulation is directly related to magma budget, then the frequency of vent fields on ultraslow ridges should be even less than that predicted by the spreading rate alone.

In the last few years, detailed plume surveys have been conducted along three long sections of ultraslow-spreading ridge: two sections of the eastern South West Indian Ridge (SWIR) between 58° and 66°E (14–16 mm/yr full rate) [*German et al.*, 1998a]; the western SWIR, 10°–23°E (8–14 mm/yr) [*Bach et al.*, 2002; *Baker et al.*, 2004]; and the Gakkel Ridge, 7°W–86°E (6–11 mm/yr) [*Edmonds et al.*, 2003]. Detailed analyses of plume and vent field distributions along these ridge sections suggest that hydrothermal activity along each is similar.

The only ultraslow ridge sections where plumes have been mapped using a continuous tow method are two segments of the eastern SWIR between 58° and 66°E [*German et al.*, 1998a]. This study located six possible hydrothermal sites using dual-pass tracks of TOBI, with an array of MAPRs spanning a 300-m-thick layer above and below the package. The TOBI data mapped laterally continuous, above-bottom optical anomalies with distinct geographical limits, strongly indicative of hydrothermal rather than erosional origins (Plate 1a). The total plume extent of 50 km within the 420 aggregate km of ridge length studied results in p_h = 0.12, consistent with a low F_s of 1.33 (Figure 5). For the 10°–23°E SWIR, p_h was calculated from the percentage of vertical MAPR profiles that recorded a plume. Of the 86 profiles collected on cruises in

2000/2001 and 2003 (Plate 1b), at least five and a maximum of 11 detected hydrothermal plumes, yielding a p_h of 0.06 to 0.13 and F_s values of 0.21–0.84 (Figure 5), although these maximum values are not tightly constrained. There is an unusually high level of uncertainty here, because Antarctic Bottom Water flowing into this section from the bounding fracture zones appears to induce widespread resuspension of bottom sediments, complicating the identification of hydrothermally derived optical anomalies [*Baker et al.*, 2004].

The Gakkel Ridge, the slowest-spreading and perhaps deepest section of the global ridge system, crosses ~1800 km of the Arctic Ocean from Greenland to Siberia. The Arctic Mid-Ocean Ridge Expedition in 2001 collected 145 MAPR profiles over 850 km of the western half of the ridge (average spacing 6.6 km), and 114 displayed light-scattering (and often temperature) anomalies characteristic of hydrothermal plumes [*Edmonds et al.*, 2003]. Calculating the p_h value either from the fraction of MAPR profiles that detected a hydrothermal plume (0.82) or from the axial plume coverage based on contouring the gridded data set (0.75, Plate 1c) yields the highest p_h yet documented on any lengthy ridge section (Figure 5b). Because of the remarkable hydrographic characteristics over the Gakkel Ridge and the unusual bathymetric characteristics of ultraslow ridges in general, however, this exceptional p_h value is not representative of the relative spatial density of hydrothermal sites. The water column below ~3500 m is effectively isopycnal within the Gakkel Ridge, allowing plumes to rise above the axial bathymetry (Plate 1c). The capacious and continuous axial valley traps many of these plumes, permitting some to disperse coherently for up to 200 km [*Edmonds et al.*, 2003; *Baker et al.*, 2004]. This situation is a cautionary lesson about the limitations of interpreting p_h in axial valleys of great relief, an even more extreme example than the Rainbow plume on the MAR, which has been traced at least 50 km downstream from its source [*German et al.*, 1998b; *Thurnherr et al.*, 2002]. Careful analysis indicates that despite an extreme p_h, only 9–10 hydrothermal fields are active on the Gakkel Ridge [*Edmonds et al.*, 2003; *Baker et al.*, 2004], so F_s = 1.1–1.2.

Adding the results from ultraslow ridges to Figure 5 shows, except for the anomalous p_h value of the Gakkel Ridge, good agreement with the trend of faster-

spreading ridges. Values for p_h on the SWIR are ~0.1 and F_s values on all three sections are ~1. V_m values for these ridges are computed using a nominal crustal thickness of 4 km [*White et al.*, 2001], though seismic observations [*Muller et al.*, 1999; *Jokat et al.*, 2003] have found thicknesses of < 2 km. Moreover, dredging and magnetic surveys of ultraslow ridges indicate that large sections may actually have near-zero crustal thickness, unless serpentinized peridotite is regarded as "crust" [*Dick et al.*, 2003]. The V_m estimates for ultraslow ridges (Table 1) are, therefore, maximum values.

The presence of ANTU plumes over both volcanic and avolcanic areas on these ridges (Plate 1) indicates that hydrothermal activity on ultraslow ridges cannot be simply related to the magmatic budget. Whereas at least six of the nine identified sites along the Gakkel Ridge occur on axial volcanic highs [*Edmonds et al.*, 2003; *Baker et al.*, 2004], sites on the SWIR appear more controlled by the tectonic environment. Enhanced permeability created by the long-lived and deeply penetrating fault planes that are a hallmark of ultraslow ridges [*Dick et al.*, 2003] can provide access to nonvolcanic heat sources such as direct cooling of the upwelling mantle and exothermic serpentinization. For example, the strongest plume on the western SWIR, at ~13.3°E (Plate 1b), was found along the wall of a large fault block with a 1200 m footwall extending from valley floor to the crest of the rift valley wall [*Bach et al.*, 2002]. Fossil hydrothermal deposits in the western SWIR were primarily found on the rift valley walls, further emphasizing the role of tectonism in controlling hydrothermal activity there [*Bach et al.*, 2002; *Dick et al.*, 2003]. On the eastern SWIR, several bathymetric highs identify locations of focused volcanism [*Münch et al.*, 2001; *Sauter et al.*, 2002; *Cannat et al.*, 2003], but at least half the detected plumes occur in the weakly volcanic zones (as determined from sidescan sonar imagery). None were observed around the summits of the major bathymetric highs [*German et al.*, 1998a]. Analyses of core-top sediments have confirmed the presence of geologically recent vent activity near plume signals at both volcanically and tectonically dominated sites on the eastern SWIR [*German*, 2003], consistent with inferences from the western SWIR that hydrothermal discharge occurs in both volcanic and nonvolcanic settings.

Clearly, we should anticipate a greater complexity in the nature of hydrothermal activity on weakly volcanic crust than would ever have been predicted from studies of fast-spreading ridges alone. Improved understanding of this aspect of heat transfer and hydrothermal circulation will only be disclosed by direct observation of seafloor processes at ultraslow-spreading ridges, a prime target for InterRIDGE-coordinated research in the future.

6. HOTSPOT-AFFECTED RIDGES

Ridge sections apparently underlain by mantle melt anomalies, or hotspots, make up an intriguing subset of the global ridge system. Three hotspot-associated ridge sections have been systematically surveyed for plume distributions: the Reykjanes Ridge from 57.75° to 63.15°N, almost a full radial transect of the Iceland hotspot; the SEIR from 35.6° to 40.2°N, a 445 km section passing over the top of the Amsterdam-St. Paul hotspot; and 35.7°–38°N on the MAR, a short section on the southern fringe of the Azores hotspot. The first two sections appear unusually deficient in hydrothermal activity compared with other sections of similar magma budget (with the exception of the 27°–30°N MAR section, of which only 50 km has been densely surveyed). *German et al.* [1994] collected 174 optical/chemical profiles using a CTDO-rosette along 750 km of the Reykjanes Ridge, at intervals of 4–18 km. Despite this intense sampling, only the Steinahóll vent field at 63.1°N was located, an F_s of only 0.013 (Figure 5a). Based on the ~10 km lateral extent to which this Steinahóll plume could be traced, these results translate to a p_h = 0.012 (Figure 5b). On the SEIR section, two certain and two possible plumes were detected on 58 MAPR profiles, corresponding to an F_s of 0.45–0.90 and a p_h value of 0.03–0.07 (Figure 5).

Mantle upwelling beneath both these ridge sections has abnormally thickened the oceanic crust to at least ~10 km [*Scheirer et al.*, 2000; *Smallwood and White*, 1998]. An early hypothesis for the Reykjanes Ridge hydrothermal results [*German et al.*, 1994, 1996c], consistent with the first sidescan sonar images of the Reykjanes Ridge [*Parson et al.*, 1993], proposed that thermal gradients beneath the present-day ridge may be sufficiently high, compared to elsewhere along the MAR, to markedly reduce the depth

of brittle fracturing of the ocean crust and consequent penetration of seawater. This hypothesis is consistent with a crustal thermal model [*Phipps Morgan and Chen*, 1993; *Chen*, 2003] that explains the combination of a shallow magma chamber at 57.74°N on the Reykjanes Ridge [*Sinha et al.*, 1997] and the lack of hydrothermal plumes [*German et al.*, 1994] as the result of a positive mantle-temperature anomaly ($\Delta T \approx 40°–70°C$) and inefficient hydrothermal cooling. The model calculations for a shallow, steady state magma chamber on a slow-spreading ridge require that convective cooling by hydrothermal discharge be only ~25% of that expected on a slow-spreading ridge not affected by a hotspot. Similar model calculations have not been run for the Amsterdam-St. Paul SEIR section, but its unusually low p_h value suggests that thickened crust there may similarly depress hydrothermal cooling.

The 35.7°–38°N section of the MAR seems to contradict this hypothesis, since F_s here is 2–3 times higher than expected for its magmatic budget (Figure 5a). A gravity analysis along this section of the MAR, however, found crustal thicknesses south of 38°N to be increased by <2 km relative to normal (~6 km) crust, shrinking to no increase south of 37°S [*Escartín et al.*, 2001]. While this area was underlain by a melt anomaly at 5–10 Ma, at present there is no crustal thickness or mantle temperature anomaly signature here [*Cannat et al.*, 1999; *Escartín et al.*, 2001]. Instead, moderate crustal thickness variations suggest magma focusing at the segment centers, especially at Lucky Strike and Menez Gwen [*Escartín et al.*, 2001]. Magma focusing, combined with fracturing of the ridge axis and establishment of short 2nd order segments linked by broad, ultramafic-exposing NTOs that accommodate the oblique orientation of the plate boundary [*Parson et al.*, 2000], may explain the relatively high F_s found here.

Determining if these results signify a systematic hotspot effect or simply a present-day sampling artifact will require a broader consideration of other hotspot-affected ridges. Of the 47 hotspots listed by *Richards et al.* [1988], only a few lie within 500 km of a ridge axis; beyond that distance hotspot influence upon ridge morphology appears negligible [*Ito and Lin*, 1995]. According to this criterion, possibly influential hotspots, besides Iceland and the St. Paul-Amsterdam system, include Galápagos, Easter, Jan Mayen, Azores, Ascension, Tristan de Cunha, Bouvet, and Crozet (Figure 1). Bouvet

and Crozet are near the ultraslow spreading SWIR where the incidence of venting is already low and so the hypothesized "hotspot effect" on venting may be difficult to discern at these locations. Tristan de Cunha is distant from the MAR axis, while the effect of the Easter Island mantle plume may be further complicated by tectonic interactions with the adjacent microplate. We conclude, therefore, that the most attractive candidates deserving of future, detailed plume/vent surveys are the Galápagos, Jan Mayen, and Ascension hotspots, together with more detailed observations around the Iceland, Azores, and Amsterdam-St. Paul hotspots.

7. DISCUSSION

7.1 Global Trends

While we have hydrothermally surveyed, to some degree, about 20% of the global ridge system (Figure 1b), only 13 ridge sections totaling half that distance (Figure 5) are suitable for examining the magmatic budget hypothesis described in the Introduction. These sections span the entire global spectrum of the ridge magmatic budget (as calculated from spreading rates), however, and describe a consistent and robust relationship. The first-order trend in plots of V_m vs. both p_h and F_s is a decline in hydrothermal activity with decreasing magma budget, though inconsistencies occur in each plot as well. In the p_h plot (Figure 5b), most of the data points (ignoring the heavily biased Gakkel Ridge data and the hotspot-affected ridges) define a robust trend with a least-squares regression of

$$p_h = 0.043 + 0.00055V_m$$

with $r^2 = 0.93$. This result agrees with earlier predictions [*Baker and Hammond, 1992*; *Baker et al., 1996*].

Considerably more scatter exists in the F_s plot (Figure 5a). We interpret this scatter as a function of three overlapping uncertainties: increasing difficulty in defining the boundaries of discrete vent fields as spreading rate increases, wide variability in the effort expended in finding discrete vent sites on different ridge sections, and pronounced differences in the length of surveyed ridge sections (Table 1). After binning these data to

mitigate these uncertainties as far as presently possible, the resultant least-squares regression is

$$F_s = 1.0 + 0.0023V_m$$

with $r^2 = 0.97$.

These robust linear relations offer sturdy support for the hypothesis that crustal magmatic budget is the primary influence on the large-scale (multisegment) distribution of hydrothermal activity. The fact that the activity on ultraslow ridges is appreciably greater than zero, especially considering that we may have conservatively overestimated the true melt supply at the sampled ridges, suggests that ultraslow ridges may in fact be more efficient producers of vent fields than other ridges. We can test this idea by normalizing F_s to the time-averaged delivery of magma [*Baker et al.*, 2004]. To normalize F_s, we calculate F_m, sites/(1000 km × Myr), for five spreading rate bins (equivalent to the magmatic budget bins in Figure 5a) as

$$F_m = 10^3 N/(Lu_s T_c)$$

where for each bin N is the number of vent fields observed, L is the total ridge length (km), u_s is the weighted average full spreading rate (mm/yr), and T_c is the nominal crustal thickness of 4 km for ultraslow ridges and 6.3 km for all other ridges [*White et al.*, 1992, 2001] (Table 1). F_m for ultraslow ridges are minimum values considering that sections of these ridges (especially where the spreading rate <12 mm/yr) may actually have near-zero crustal thickness [*Dick et al.*, 2003]. F_m steadily increases from superfast to slow ridges then increases sharply for ultraslow ridges (Figure 7). For a given magmatic budget, ultraslow ridges appear 2–4 times as efficient as fast-spreading ridges in creating vent fields. The trend of increasing F_m with decreasing u_s is consistent with the expected addition of heat from sources other than crustal cooling of basaltic magma at slow and ultraslow ridges. We caution again, though, that data from slow ridges is uncomfortably scarce.

Additional work on slow and ultraslow ridges will be required to establish whether the apparent trend between F_m and u_s can be verified. In particular, the data for slow (20–55 mm/yr) ridges are so limited that our calculated F_m is speculative. If this trend is confirmed by future surveys, it will indicate that as spreading rates decrease the incidence of hydrothermal activity can be increased by factors other than the long-term magmatic budget. These may include an increased bulk permeability effected by the penetration of deep and enduring faults, strongly three-dimensional magma delivery, and additional heat sources such as direct cooling of the upper mantle, cooling gabbroic intrusions, and serpentinization.

Despite the robust trends in Figure 5, it is important to remember that these results do not demand that the fluxes of hydrothermal heat or chemicals are also similarly related to the magmatic budget. Many additional quantitative flux measurements, at a variety of spreading rates, will be needed to confirm that inference.

The global trend established in Figure 5a can also be used to estimate the total number of vent fields presently active on the ridge system. If we recast the binned data in Figure 5a as a plot of F_s vs. u_s, the least-squares regression is

$$F_s = 0.88 + 0.015u_s.$$

Applying this relation to the global distribution of ridge spreading rates binned at 20 mm/yr intervals yields a histogram of predicted vent sites with a total population of 1060 (with 95% confidence limits of 992–1153) (Figure 8). In contrast to the dominance of slow-spreading ridges in the global distribution of spreading rates (Figure 2c), vent field populations differ by only about a factor of 2 across spreading rate categories, except in the 100–140 mm/yr bins where total ridge length is <2% of the global sum.

7.2 A Millennial-Scale View of Global Hydrothermal Venting

A recurring concern in attempting to relate hydrothermal activity to geological variability is that hydrothermal data are unavoidably time aliased. Mean hydrothermal

activity over a much longer period might be distributed quite differently than at present, especially at slow spreading rates. This problem can be partially addressed by comparing the vent field distribution with the oceanic distribution of ^{3}He, an unequivocal and conservative tracer of magmatic degassing along ridge crests [*Craig and Lupton*, 1981]. Overlaying the global ridge system with the deep-water (2000–3000 m) (δ^3He%) pattern [*Geosecs Atlantic, Pacific, and Indian Ocean Expeditions*, 1987; *Jamous et al.*, 1992; *Lupton*, 1995, 1998; *Rüth et al.*, 2000] reveals a strong, but not perfect, correlation between u_s and $\delta(^3$He%) (Figure 9). The most intense $\delta(^3$He%) plume in the ocean spreads westward from the fastest spreading ridge segments in the ocean, and other intense plumes originate on the fast-spreading northern EPR and the intermediate-rate JDFR. The Atlantic has lower $\delta(^3$He%) than either the Pacific or Indian Oceans [*Geosecs Atlantic, Pacific, and Indian Ocean Expeditions*, 1987; *Rüth et al.*, 2000]. This general pattern suggests that we have not grossly misrepresented the differences in hydrothermal activity between fast- and slow-spreading ridges, and demonstrates that this relation holds over at least the last ~10^3 yr. This timescale is equivalent to both the turnover time of the oceans' thermohaline circulation and, coincidentally, the time for a water volume equal to the global ocean to be cycled through hydrothermal plumes [*Kadko et al.*, 1995; German et al., preprint, 2004].

Past this basic distinction between fast and slow ridges in Figure 9, the distribution of $\delta(^3$He%) becomes more complex. Values of $\delta(^3$He%) along fast-spreading ridges in the eastern Pacific show discrete highs rather than a uniform distribution corresponding to the spreading rate trend. Unexpectedly low $\delta(^3$He%) values occur all along the ridge from the Indian Ocean triple junction to the EPR-Chile Rise triple junction. These features are not solely the result of long-wavelength fluctuations in the distribution of vent fields, but instead may be generated by patterns of oceanographic advection and ventilation. Deep currents in the eastern Pacific and vigorous vertical and circumpolar mixing around Antarctica are two primary controls on the $\delta(^3$He%) distribution [*Farley et al.*, 1995; *Lupton*, 1998]. These complications, in fact, emphasize the value of more complete knowledge about the global distribution of vent fields.

Without accurate knowledge of ^{3}He sources along the global ridge system, the utility of δ(^{3}He%) distributions as a tracer of ocean advection and mixing will remain limited.

8. CONCLUSIONS

In the last quarter-century we have progressed from the discovery of vent fields, to conceptually straightforward hydrothermal surveys along many fast-spreading ridges, to the challenge of cataloging hydrothermal activity throughout Earth's oceans. This progress allows us to test, on a global scale, the proposition that hydrothermal activity increases linearly with the magmatic budget. About 20% of the ~67,000 km global ridge system has now been explored, to some degree, for hydrothermal venting, along with ~3000 km of submarine volcanic arcs and a few intraplate volcanoes. We can precisely locate ~145 confirmed vent sites and have indications of another ~130 based on water column observations alone. Fast ridges (no rift valley), spreading at full rates >55 mm/yr, presently account for 125 sites, slow ridges (rift valley, 20–55 mm/yr) for 55 sites, and ultraslow ridges (<20 mm/yr) for 34 sites. Vent site exploration has long been focused in the eastern Pacific and northern Atlantic ridges. Along a 30,000 km span of ridge from the equatorial Mid-Atlantic Ridge, through the Indian Ocean, to 38°S on the East Pacific Rise we know of only two confirmed sites, separated by <150 km, although more than 20 further likely targets have been identified from plume studies. If our present distribution of sites is representative across all spreading rates, then the expected total global population of active vent fields on the ridge system is ~1000.

Of the explored ridge, on only 13 sections totaling ~7400 km do we have reasonable confidence in our estimates of the relative frequency of hydrothermal activity. Using either plume incidence, p_h, or site frequency, F_s, and regressing the estimates from each section (except two hotspot-affected ridge sections) against the crustal magmatic budget, V_m, yields statistically robust linear trends spanning spreading rates from 10–150 mm/yr. These direct correlations are consistent with the hypothesis that V_m, rather than any spreading-rate-dependent variability in the bulk crustal permeability, for example, is the principal control on the distribution of hydrothermal activity. This conclusion is

supported by the oceanic pattern of deep $\delta(^3He\%)$, an unequivocal hydrothermal indicator, which agrees with a ridge source distribution that is a function of spreading rate.

In addition to this first-order trend, the data also suggest that ultraslow and slow ridges support 2–4 times as many vent sites, for a given V_m, than do faster ridges. We interpret this result as an indication that ultraslow ridges, as well as slow ridges to a lesser degree, use deep and enduring faults, strongly three-dimensional magma delivery, and additional heat sources such as direct cooling of the upper mantle, cooling gabbroic intrusions, and serpentinization to supplement the heat supplied by the crustal cooling of basaltic melt.

It is important to remember that these conclusions assume that the average vent field heat flux does not vary systematically with spreading rate. While flux measurements are rare and arduous to obtain, the steady accumulation of information on the tectonic setting, size, and nature of vent fields will eventually permit a reliable test of this assumption.

What are some of the critical problems that call for our attention in the next decade? Several key questions evolve from this review:

1. Are the geologic processes that control venting on slow ridges more similar to those on fast ridges or ultraslow ridges? Slow ridges have fewer systematic hydrothermal surveys than any other ridge type (~10% of their total length), and none suitable for calculating p_h. The question of magmatic vs. tectonic control is still an open one. Current "volcanic-tectonic-hydrothermal cycle" models are based on studies at fast ridges and require testing in other environments. Our inventory of surveys along slow-spreading ridges needs considerable expansion.

2. Are hotspot-affected ridge sections systematically deficient in convective hydrothermal cooling compared to other sections of similar spreading rate? Additional work at the Reykjanes Ridge and more comprehensive surveys over the Galápagos and Azores hotspots are needed. Surveys of discovery should be conducted over hotspots such as Galápagos, Jan Mayan, and Ascension.

3. Is heat from sources other than crustal cooling of basalt melt an important contributor to hydrothermal circulation at ultraslow ridges? If so, does it materially influence the fluid chemistry and ecology of these sites?

4. Will surveys along the contiguous half of the global ridge that is virtually unexplored support the conclusions presented here? Exploration, spurred by such fundamental questions as vent biogeography, should remain a key objective of InterRIDGE investigators. Back-arc basins such as the Lau Basin and the Mariana Trough, where spreading rates often vary substantially along axis over comparatively short distances, also remain under-surveyed to-date.

With continued attention to both spatial and temporal variability, perhaps in another decade we can derive a confident and quantitative relationship between hydrothermal activity and the magmatic budget at ridges of all types.

Acknowledgments. This review was supported by the NOAA VENTS Program (ETB) and by NERC (CRG). We expressly acknowledge the countless colleagues who have contributed time and energy into the collection of these data. The impetus for this paper was the 2001 InterRIDGE Theoretical Institute at the University of Pavia in Italy. We thank the conveners and participants for channeling our energies into this effort. Thanks also to helpful reviews from R. Haymon, L. Parson, and J. Lin. PMEL contribution number 2544.

REFERENCES

Aballéa, M., J. Radford-Knoery, P. Appriou, H. Bogault, J. L. Charlou, J. P. Donval, J. Etoubleau, Y. Fouquet, C. R. German, and M. Miranda, Manganese distribution in the water column near the Azores Triple Junction along the Mid-Atlantic Ridge and in the Azores domain, *Deep-Sea Res. I, 45*, 1319–1338, 1998.

A.P.H.A. (American Public Health Assoc.), *Standard Methods for the Examination of Water and Wastewater*, 16th ed. A.P.H.A., A.W.W.A, and W.P.C.F. joint publication, Washington D.C., 1268 pp., 1985.

Auzende, J.-M., V. Ballu, R. Batiza, D. Bideau, J.-L. Charlou, M. H. Cormier, Y. Fouquet, P. Geistdoerfer, Y. Lagabrielle, J. Sinton, and P. Spadea, Recent tectonic, magmatic, and hydrothermal activity on the East Pacific Rise between 17°S and 19°S: Submersible observations, *J. Geophys. Res., 101*, 17,995–18,010, 1996.

Bach, W., N. R. Banerjee, H. J. B. Dick, and E. T. Baker, Discovery of ancient and active hydrothermal systems along the ultra-slow spreading Southwest Indian Ridge, 10°–16°E, *Geochem. Geophys. Geosyst., 3*, 2001GC000279, 2002.

Baker, E. T., and S. R. Hammond, Hydrothermal venting and the apparent magmatic budget of the Juan de Fuca Ridge, *J. Geophys. Res., 97*, 3443–3456, 1992.

Baker, E. T., and G. J. Massoth, Characteristics of hydrothermal plumes from two vent fields on the Juan de Fuca Ridge, northeast Pacific Ocean, *Earth Planet. Sci. Lett., 85*, 59–73, 1987.

Baker, E. T., and H. B. Milburn, MAPR: A new instrument for hydrothermal plume mapping, *RIDGE Events, 8*, 23–25, 1997.

Baker, E. T., and T. Urabe, Extensive distribution of hydrothermal plumes along the superfast-spreading East Pacific Rise, 13°50′–18°40′S, *J. Geophys. Res., 101*, 8685–8695, 1996.

Baker, E. T., J. W. Lavelle, and G. J. Massoth, Hydrothermal particle plumes over the southern Juan de Fuca Ridge, *Nature, 316*, 342–344, 1985.

Baker, E. T., R. A. Feely, M. J. Mottl, F. J. Sansone, C. G. Wheat, J. A. Resing, and J. E. Lupton, Hydrothermal plumes along the East Pacific Rise, 8°40′ to 11°50′N: Plume distribution and relationship to the apparent magmatic budget, *Earth Planet. Sci. Lett., 128*, 1–17, 1994.

Baker, E. T., C. R. German, and H. Elderfield, Hydrothermal plumes over spreading-center axes: Global distributions and geological inferences, in *Seafloor Hydrothermal Systems: Physical, Chemical, Biological, and Geological Interactions, Geophys. Monogr. Ser., 91*, edited by S. Humphris, R. Zierenberg, L. S. Mullineaux, and R. Thomson, pp. 47–71, AGU, Washington D.C., 1995.

Baker, E. T., Y. J. Chen, and J. Phipps Morgan, The relationship between near-axis hydrothermal cooling and the spreading rate of midocean ridges, *Earth Planet. Sci. Lett., 142*, 137–145, 1996.

Baker, E. T., M.-H. Cormier, C. H. Langmuir, and K. Zavala, Hydrothermal plumes along segments of contrasting magmatic influence, 15°20′–18°30′N, East Pacific Rise: Influence of axial faulting, *Geochem. Geophys. Geosyst., 2*, doi:2000GC000165, 2001b.

Baker, E. T., D. A. Tennant, R. A. Feely, G. T. Lebon, and S. L. Walker, Field and laboratory studies on the effect of particle size and composition on optical backscattering measurements in hydrothermal plumes, *Deep-Sea Res. I, 48*, 593–604, 2001a.

Baker, E. T., R. N. Hey, J. E. Lupton, J. A. Resing, R. A. Feely, J. J. Gharib, G. J. Massoth, F. J. Sansone, M. Kleinrock, F. Martinez, D. F. Naar, C. Rodrigo, D.

Bohnenstiehl, and D. Pardee, Hydrothermal venting along Earth's fastest spreading center: East Pacific Rise, 27.5°–32.3°S, *J. Geophys. Res., 107*, doi:10.1029/2001JB000651, 2002.

Baker, E. T., H. N. Edmonds, P. J. Michael, W. Bach. H. J. B. Dick, J. E. Snow, S. L. Walker, N. R. Banerjee, and C. H. Langmuir, Hydrothermal venting in magma deserts: The ultraslow-spreading Gakkel and South West Indian Ridges, *Geochem., Geophys., Geosyst., 5*(8), Q08002, doi:10.1029/2004GC000712, 2004.

Barriga, F. J. A. S., Y. Fouquet, A. Almeida, M. Biscoito, J.-L. Charlou, R. L. P. Costa, A. Dias, A. M. S. F. Marques, J. M. A. Miranda, K. Olu, F. Porteiro, M. G. P. S. Queiroz, Discovery of the Saldanha Hydrothermal Field on the FAMOUS Segment of the MAR (36°30'N), *Eos Trans. AGU, 79*(45), Fall Meet. Suppl., F67, 1998.

Bird, P., An updated digital model of plate boundaries, *Geochem. Geophys. Geosyst., 4*, 1027, doi:10.1029/ 2001GC000252, 2003.

Boström, K., M. N. A. Peterson, O. Joensuu, and D. E. Fisher, Aluminum-poor ferromangoan sediments on active ocean ridges, *J. Geophys. Res*., 74, 3261–3270, 1969.

Bougault, H., J. L. Charlou, Y. Fouquet, and H. D. Needham, Activité hydrothermale et structure axiale des dorsales Est-Pacifique et médio-Atlantique, *Oceanol. Acta, vol. special 10*, 199–207, 1990.

Bougault, H., M. Aballéa, J. Radford-Knoery, J. L. Charlou, P. Jean Baptiste, P. Appriou, H. D. Needham, C. German, and M. Miranda, FAMOUS and AMAR segments on the Mid-Atlantic Ridge: ubiquitous hydrothermal Mn, CH_4, δ^3He signals along the rift valley walls and rift offsets, *Earth Planet. Sci. Lett., 161*, 1–17, 1998.

Cannat, M., A. Briais, C. Deplus, J. Escartín, J. Georgen, J. Lin, S. Mercouriev, C. Meyzen, M. Muller, G. Pouliquen, A. Rabain, and P. da Silva, Mid-Atlantic Ridge-Azores hotspot interactions: along-axis migration of a hotspot-derived event of enhanced magmatism 10 to 3 Ma ago, *Earth Planet. Sci. Lett., 173*, 257–269, 1999.

Cannat, M., C. Rommevaux-Jestin, and H. Fujimoto, Melt supply variations to a magma-poor ultra-slow spreading ridge (Southwest Indian Ridge 61° to 69°E), *Geochem. Geophys. Geosyst., 4,* 9104, doi:10.1029/2002GC000480, 2003.

Cannat, M., J. Cann, and J. Maclennan, Some hard rock constraints on the supply of heat to mid-ocean ridges, in *Mid-ocean ridges: Hydrothermal interactions between the lithosphere and oceans, Geophys. Monogr. Ser.,* vol. 148, edited by C. German, J. Lin, and L. Parson, AGU, Washington, D.C., 111-150, 2004.

Charlou, J. L., and J.-P. Donval, Hydrothermal methane venting between 12°N and 26°N along the Mid-Atlantic Ridge, *J. Geophys. Res., 98*, 9625–9642, 1993.

Charlou, J. L., H. Bougault, P. Appriou, T. Nelsen, and P. Rona, Different TDM/CH_4 hydrothermal plume signatures: TAG site at 26°N and serpentinized ultrabasic daipir at 15°05'N on the Mid-Atlantic Ridge, *Geochim. Cosmochim. Acta, 55*, 3209–3222, 1991.

Charlou, J. L., J. P. Donval, Y. Fouquet, P. Jean-Baptiste, and N. Holm, Geochemistry of high H_2 and CH_4 vent fluids issuing from ultramafic rocks at the Rainbow hydrothermal field (36°14'N, MAR), *Chem. Geol., 191*, 345–359, 2002.

Chen Y. J., Influence of the Iceland mantle plume on crustal accretion at the inflated Reykjanes Ridge: Magma lens and low hydrothermal activity?, *J. Geophys. Res., 108*(B11), 2524, doi:10.1029/ 2001JB000816, 2003.

Chin, C. S., G. P. Klinkhammer, and C. Wilson, Detection of hydrothermal plumes on the Northern Mid-Atlantic Ridge: results from optical measurements, *Earth Planet. Sci. Lett., 162*, 1–13, 1998.

Corliss, J. B., J. Dymond, L. I. Gordon, J. M. Edmond, R. P. von Herzen, R. D. Ballard, K. Green, D. Williams, A. Bainbridge, K. Crane, and T. H. van Andel, Submarine thermal springs on the Galápagos Rift, *Science, 203*, 1073–1083, 1979.

Craig, H., and J. E. Lupton, Helium-3 and mantle volatiles in the ocean and the oceanic crust, in *The Sea*, edited by C. Emiliani, New York, Wiley, *7*, 391–428, 1981.

Crane, K., F.A. Aikman III, R. Embley, S. Hammond, A. Malahoff, and J. Lupton, The distribution of geothermal fields on the Juan de Fuca Ridge, *J. Geophys. Res., 90*, 727–744, 1985.

DeMets, C., R. G. Gordon, D. F. Argus, and S. Stein, Current plate motions, *Geophys. J. Int., 101*, 425–478, 1990.

de Ronde, C. E. J., G. J. Massoth, E. T. Baker, and J. E. Lupton, Submarine hydrothermal venting related to volcanic arcs, Giggenbach Memorial Volume, in *Volcanic, geothermal and ore-forming fluids: Rulers and witnesses of processes within the Earth*, edited by S. F. Simmons and I. Graham, *Soc. of Econ. Geolog., 10*, 91–110, 2003.

Dick, H. J. B., J. Lin, and H. Schouten, An ultraslow-spreading class of ocean ridge, *Nature, 426*, 405–412, 2003.

Douville, E., J. L. Charlou, E. H. Oelkers, P. Bienvenu, C. F. J. Colon, J. P. Donval, Y. Fouquet, D. Prieur, and P. Appriou, The rainbow vent fluids (36°14 N, MAR): the influence of ultramafic rocks and phase separation on trace metal content in Mid-Atlantic Ridge hydrothermal fluids, *Chem. Geol., 184*, 37–48, 2002.

Edmonds, H. N., P. J. Michael, E. T. Baker, D. P. Connelly, J. E. Snow, C. H. Langmuir, H. J. B. Dick, R. Mühe, C. R. German, and D. W. Graham, Discovery of abundant

hydrothermal venting on the ultraslow-spreading Gakkel Ridge, Arctic Ocean, *Nature, 421*, 252–256, 2003.

Embley, R. W., J. E. Lupton, G. Massoth, T. Urabe, V. Tunnicliffe, D. A. Butterfield, T. Shibata, O. Okano, M. Kinoshita, and K. Fujioka, Geological, chemical, and biological evidence for recent volcanism at 17.5°S: East Pacific Rise, *Earth Planet. Sci. Lett., 163*, 131–147, 1998.

Embley, R. W., E. T. Baker, W. W. Chadwick, Jr., J. E. Lupton, J. A. Resing, G. J. Massoth, and K. Nakamura, Explorations of Mariana Arc volcanoes reveal new hydrothermal systems, *Eos Trans. AGU, 85*(4), 37, 40, 2004.

Escartín, J., M. Cannat, G. Pouliquen, and A. Rabain, Crustal thickness of V-shaped ridges south of the Azores: Interaction of the Mid-Atlantic Ridge (36°–39°N) and the Azores hot spot, *J. Geophys. Res., 106*, 21,719–21,735, 2001.

Farley, K. A., E. Maier-Reimer, P. Schlosser, and W. S. Broecker, Constraints on mantle ^{3}He fluxes and deep-sea circulation from an oceanic general circulation model, *J. Geophys. Res., 100*, 3829–3839, 1995.

Fisher, A. T., Permeability within basaltic oceanic crust, *Rev. Geophys., 36*, 143–182, 1998.

Fouquet, Y., H. Ondréas, J.-L. Charlou, J.-P. Donval, J. Radford-Knoery, I. Costa, N. Lourenço, and M. K. Tivey, Atlantic lava lakes and hot vents, *Nature, 377*, 201, 1995.

Fouquet, Y., J. L. Charlou, H. Ondréas, J. Radford-Knoery, J. P. Donval, E. Douville, R. Apprioual, P. Cambon, H. Pell, J. Y. Landur, and A. Normand, Discovery and first submersible investigations on the Rainbow hydrothermal field on the MAR (36°14′N), *Eos Trans. AGU, 78*(46), Fall Meet. Suppl., F832, 1997.

Fouquet, Y., J. L. Charlou, and F. Barriga, Modern seafloor hydrothermal deposits hosted in ultramafic rocks, *Geol. Soc. Am. Abstracts with Programs, 34*(6), A 194–7, 2002.

Francheteau, J., and R. Ballard, The East Pacific Rise near 21°N, 13°N and 20°S: inferences for along-strike variability of axial processes of the Mid-Ocean Ridge, *Earth Planet. Sci. Lett., 64*, 93–116, 1983.

Geosecs Atlantic, Pacific, and Indian Ocean Expeditions, 7, Shorebased Data and Graphics, National Science Foundation, U.S. Govt. Print. Office, Washington, D.C., 1987.

German, C. R., Hydrothermal activity on the eastern SWIR (50°-70°E): Evidence from core-top geochemistry, 1887 and 1998, *Geochem. Geophys. Geosyst., 4*(7), 9102 doi:10.1029/2003GC000522, 2003.

German, C. R., and L. M. Parson, Distributions of hydrothermal activity along the Mid-Atlantic Ridge: Interplay of magmatic and tectonic controls, *Earth. Planet. Sci. Lett., 160*, 327–341, 1998.

German, C. R., J. Briem, C. Chin, M. Danielsen, S. Holland, R. James, A. Jónsdóttir, E. Ludford, C. Moser, J. Olafsson, M. R. Palmer, and M. D. Rudnicki, Hydrothermal activity on the Reykjanes Ridge: The Steinahóll Vent-field at 63°06′N, *Earth Planet. Sci. Lett., 121*, 647–654, 1994.

German, C. R., E. T. Baker, and G. Klinkhammer, The regional setting of hydrothermal activity, in *Hydrothermal Vents and Processes*, edited by L. M. Parson, C. L. Walker, and D. R. Dixon, *Geol. Soc. Spec. Pub. No. 87*, 3–15, 1995.

German, C. R., L. M. Parson, and HEAT Scientific Team, Hydrothermal exploration at the Azores Triple-Junction: Tectonic control of venting at slow-spreading ridges?, *Earth Planet. Sci. Lett., 138*, 93–104, 1996a.

German C. R., G. P. Klinkhammer, and M. D. Rudnicki, The Rainbow hydrothermal plume, 36°15′N, MAR, *Geophys. Res. Lett., 23*, 2979–2982, 1996b.

German, C. R., L. M. Parson, B. J. Murton, and H. D. Needham, Hydrothermal activity and ridge segmentation on the Mid-Atlantic Ridge: A tale of two hot-spots? in *Ridge Segmentation*, edited by C. McLeod, C. L. Walker and P. Tyler, *Geol. Soc. Spec. Pub. 118*, 169–184, 1996c.

German, C. R., E. T. Baker, C. Mevel, K. Tamaki, and the FUJI Scientific Team, Hydrothermal activity along the southwest Indian Ridge, *Nature, 395*, 490–493, 1998a.

German, C. R., K. J. Richards, M. D. Rudnicki, M. M. Lam, J. L. Charlou, and FLAME Scientific Party, Topographic control of a dispersing hydrothermal plume, *Earth Planet. Sci. Lett., 156*, 267–273, 1998b.

German, C. R., M. D. Rudnicki, and G. P. Klinkhammer, A segment-scale survey of the Broken Spur hydrothermal plume, *Deep-Sea Res. I, 46*, 701–714, 1999.

German, C. R., D. P. Connelly, A. J. Evans, L. M. Parson, Hydrothermal activity on the southern Mid-Atlantic Ridge, *Eos Trans. AGU, 83*(47), Fall Meet. Suppl., Abstract V61B–1361, 2002.

Gràcia, E., J. L. Charlou, J. Radford-Knoery, and L. M. Parson, Non-transform offsets along the Mid-Atlantic Ridge south of the Azores (38°N–34°N): ultramafic exposures and hosting of hydrothermal vents, *Earth Planet. Sci. Lett., 177*, 89–103, 2000.

Grindlay, N. R., J. A. Madsen, C. Rommevaux-Jestin, and J. Sclater, A different pattern of ridge segmentation and mantle Bouguer gravity anomalies along the ultra-slow

spreading Southwest Indian Ridge (15°30′E to 25°E), *Earth Planet. Sci. Lett., 161*, 243–253, 1998.

Haymon, R.M., The response of ridge-crest hydrothermal systems to segmented, episodic magma supply, in *Tectonic, Magmatic, Hydrothermal, and Biological Segmentation of Mid-Ocean Ridges*, edited by C. J. MacLeod, P. A. Tyler, and C. L. Walker, *Geol. Soc. Spec. Pub. 118*, 157–168, 1996.

Haymon, R. M., D. J. Fornari, M. H. Edwards, S. Carbotte, D. Wright, and K. C. Macdonald, Hydrothermal vent distribution along the East Pacific Rise crest (9°09′–54′N) and its relationship to magmatic and tectonic processes on fast-spreading mid-ocean ridges, *Earth Planet. Sci. Lett., 104*, 513–534, 1991.

Haymon, R. M. et al., Distribution of fine-scale hydrothermal, volcanic, and tectonic features along the EPR crest, 17°15′–18°30′S: Results of near-bottom acoustic and optical surveys, *Eos Trans. AGU, 78*(46), Fall Meet. Suppl., Abstract F705, 1997.

Holm, N. G., and J.-L. Charlou, Initial indications of abiotic formation of hydrocarbons in the Rainbow ultramafic hydrothermal system, Mid-Atlantic, *Earth Planet. Sci. Lett., 191*, 1–8, 2001.

Ishibashi, J., and T. Urabe, Hydrothermal activity related to arc-backarc magmatism in the western Pacific, in *Backarc Basins: Tectonics and Magmatism*, edited by B. Taylor, pp. 451–495, Plenum Press, New York, 1995.

Ito, G., and J. Lin, Oceanic spreading center-hotspot interactions: Constraints from along-isochron bathymetric and gravity anomalies, *Geology, 23*, 657–660, 1995.

Jamous, D., L. Mémery, C. Andrié, P. Jean-Baptiste, and L. Merlivat, The distribution of helium 3 in the deep western and southern Indian Ocean, *J. Geophys. Res., 97*, 2243–2250, 1992.

Jokat, W., O. Ritzmann, M. C. Schmidt-Aursch, S. Drachev, S. Gauger, and J. Snow, Geophysical evidence for reduced melt production on the Arctic ultraslow Gakkel mid-ocean ridge, *Nature, 423*, 962–965, 2003.

Kadko, D., J. Baross, and J. Alt, The magnitude and global implications of hydrothermal flux, in *Seafloor Hydrothermal Systems: Physical, Chemical, Biological, and Geological Interactions, Geophys. Monogr. Ser., 91*, edited by S. Humphris, R. Zierenberg, L. S. Mullineaux, and R. Thomson, pp. 446–466, AGU, Washington D.C., 1995.

Kelemen, P., Igneous crystallization beginning at 20 km beneath the Mid-Atlantic Ridge, 14°–16°N, *Eos Trans. AGU, 84*(46), Fall Meet. Suppl., Abstract V22H-03, 2003.

Kelley, D. S., J. A. Karson, D. K. Blackman, G. Fruh-Green, J. Gee, D. A. Butterfield, M. D. Lilley, E. J. Olson, M. O. Schrenk, K. K. Roe, G. Lebon, P. Rizzigno, J. Cann, B. John,

D. K. Ross, S. Hurst, and G. Sasagawa, An off-axis hydrothermal vent field near the Mid-Atlantic Ridge at 30°N, *Nature, 412*, 145–149, 2001.

Klinkhammer, G., P. Rona, M. Greaves, and H. Elderfield, Hydrothermal manganese plumes in the mid-Atlantic Ridge rift valley, *Nature, 314*, 727–731, 1985.

Klinkhammer, G., H. Elderfield, M. Greaves, P. Rona, and T. Nelsen, Manganese geochemistry near high-temperature vents in the Mid-Atlantic rift valley, *Earth Planet. Sci. Lett., 80*, 230–240, 1986.

Krasnov, S. G., G. A. Cherkashev, T. V. Stepanova, B. N. Batuyev, A. G. Krotov, B. V. Malin, M. N. Maslov, V. F. Markov, I. M. Poroshina, M. S. Samovarov, A. M. Ashadze, and I. K. Eromlayev, Detailed geographical studies of hydrothermal fields in the North Atlantic, in *Hydrothermal Vents and Processes*, edited by L. M. Parson, C. L. Walker, and D. R. Dixon, *Geol. Soc. Spec. Pub. 87*, 43–64, 1995.

Langmuir, C. H., D. Fornari, D. Colodner, J.-L. Charlou, I. Costa, D. Desbruyeres, D. Desonie, T. Emerson, A. Fiala-Medioni, Y. Fouquet, S. Humphris, L. Saldanha, R. Sours-Page, M. Thatcher, M. Tivey, C. Van Dover, K. Von Damm, K. Weiss, and C. Wilson, Geological setting and characteristics of the Lucky Strike Vent Field at 37°17′N on the Mid-Atlantic Ridge, *Eos, Trans. AGU, 74* (Fall Supplement), 99, 1993.

Lowell, R. P., and P. A. Rona, Seafloor hydrothermal systems driven by the serpentinization of peridotite, *Geophys. Res. Lett., 29*, doi:10.1029/2001GL014411, 2002.

Lupton, J. E., Hydrothermal plumes: Near and far field, in *Seafloor Hydrothermal Systems: Physical, Chemical, Biological, and Geological Interactions, Geophys. Monogr. Ser., 91*, edited by S. Humphris, R. Zierenberg, L. S. Mullineaux, and R. Thomson, pp. 317–346, AGU, Washington D.C., 1995.

Lupton, J. E., Hydrothermal helium plumes in the Pacific Ocean, *J. Geophys. Res., 103*, 15,853–15,868, 1998.

Lupton, J. E., J.-I. Ishibashi, and D. A. Butterfield, Gas chemistry of hydrothermal fluids along the southern East Pacific Rise, 13.5°–18.5°S, *Eos Trans. AGU, 78*(46), Fall Meet. Suppl., F706, 1997.

Lupton, J. E., D. Butterfield, M. Lilley, J.-I. Ishibashi, D. Hey, and L. Evans, Gas chemistry of hydrothermal fluids along the East Pacific Rise, 5°S to 32°S, *Eos Trans. AGU, 80*(46), Fall Meet. Suppl., F1099, 1999.

Michael, P. J., C. H. Langmuir, H. J. B. Dick, J. E. Snow, S. L. Goldstein, D. W. Graham, K. Lehnert, G. Kurras, W. Jokat, R. Mühe, and H. N. Edmonds, Magmatic and amagmatic seafloor generation at the ultraslow-spreading Gakkel Ridge, Arctic Ocean, *Nature, 423*, 956–961, 2003.

Muller, M. R., T. A. Minshull, and R. S. White, Segmentation and melt supply at the Southwest Indian Ridge, *Geology, 27*, 867–870, 1999.

Münch, U., C. Lalou, P. Halbach, and H. Fujimoto, Relict hydrothermal events along the super-slow Southwest Indian spreading ridge near 63°56′E—mineralogy, chemistry and chronology of sulfide samples, *Chem. Geol., 177*, 341–349, 2001.

Murton, B. J., G. Klinkhammer, K. Becker, A. Briais, D. Edge, N. Hayward, N. Millard, I. Mitchell, I. Rouse, M. Rudnicki, K. Sayanagi, H. Sloan, and L. Parson, Direct evidence for the distribution and occurrence of hydrothermal activity between 27°N–30°N on the Mid-Atlantic Ridge, *Earth Planet. Sci. Lett., 125*, 119–128, 1994.

Nelsen, T. A., G. P. Klinkhammer, J. H. Trefrey, and R. P. Trocine, Real-time observations of dispersed hydrothermal plumes using nephelometry: examples from the Mid-Atlantic Ridge, *Earth. Planet. Sci. Lett., 81*, 245–252, 1986/87.

ODP (Ocean Drilling Program) Leg 106 Scientific Party, Drilling the Snake Pit hydrothermal sulfide deposit on the Mid-Atlantic Ridge, Lat. 23°N, *Geology, 14*, 1004–1007, 1986.

Parson, L. M., B. J. Murton, R. C. Searle, D. Booth, J. Evans, P. Field, J. Keeton, A. Laughton, E. McAllister, N. Millard, L. Redbourne, I. Rouse, A. Shor, D. Smith, S. Spencer, C. Summerhayes, and C. Walker, En-echelon axial volcanic ridges at the Reykjanes Ridge—A life-cycle of volcanism and tectonics, *Earth Planet. Sci. Lett., 117*, 73–87, 1993.

Parson L., E. Gràcia, D. Coller, C. German, and D. Needham, Second-order segmentation; the relationship between volcanism and tectonism at the MAR, 38°N–35°40′N, *Earth Planet. Sci. Lett., 178*, 231–251, 2000.

Phipps Morgan, J., and Y. J. Chen, The genesis of oceanic crust: Magma injection, hydrothermal circulation, and crustal flow, *J. Geophys. Res., 98*, 6283–6297, 1993.

Reid, I., and H. R. Jackson, Oceanic spreading rate and crustal thickness, *Mar. Geophys. Res., 5*, 165–172, 1981.

Renard, V., R. Hekinian, J. Francheteau, R. D. Ballard, and H. Backer, Submersible observations at the axis of the ultra-fast-spreading East Pacific Rise (17°30′ to 21°30′S), *Earth Planet. Sci. Lett., 75*, 339–353, 1985.

Richards, M. A., B. H. Hager, and N. H. Sleep, Dynamically supported geoid highs over hotspots: Observation and theory, *J. Geophys. Res., 93*, 7690–7708, 1988.

Rona, P. A., G. Klinkhammer, T. A. Nelsen, J. H. Trefry, and H. Elderfield, Black smokers, massive sulfides and vent biota at the mid-Atlantic Ridge, *Nature, 321*, 33–37, 1986.

Rüth, C., R. Well, and W. Roether, Primordial ^{3}He in South Atlantic deep waters from sources on the Mid-Atlantic Ridge, *Deep-Sea Res. I, 47*, 1059–1075, 2000.

Sauter, D., L. Parson, V. Mendel, C. Rommevaux-Jestin, O. Gomez, A. Briais, C. Mevel, and K. Tamaki, TOBI sidescan sonar imagery of the very slow-spreading Southwest Indian Ridge: evidence for along-axis magma distribution, *Earth Planet. Sci. Lett., 202*, 511–512, 2002.

Scheirer, D. S., E. T. Baker, and K. T. M. Johnson, Detection of hydrothermal plumes along the Southeast Indian Ridge near the Amsterdam-St. Paul hotspot, *Geophys. Res. Lett., 25*, 97–100, 1998.

Scheirer, D. S., D. W. Forsyth, J. A. Conder, M. A. Eberle, S.-H. Hung, K. T. M. Johnson, and D. W. Graham, Anomalous seafloor spreading of the Southeast Indian Ridge near the Amsterdam-St. Paul Plateau, *J. Geophys. Res., 105*, 8243–8262, 2000.

Schroeder, T., B. John, and B. R. Frost, Geologic implications of seawater circulation through peridotite exposed at slow-spreading ridges, *Geology, 30*, 367–370, 2002.

Sinha, M. C., D. A. Navin, L. M. MacGregor, S. Constable, C. Peirce, A. White, G. Heinson, and M. A. Inglis, Evidence for accumulated melt beneath the slow-spreading Mid-Atlantic ridge, *Phil. Trans. R. Soc. Lond. A, 355*, 233–253, 1997.

Smallwood, J. R., and R. S. White, Crustal accretion at the Reykjanes Ridge, 61°–62°N, *J. Geophys. Res., 103*, 5185–5201, 1998.

Thurnherr, A. M., K. J. Richards, C. R. German, G. F. Lane-Serff, and K. G. Speer, Flow and mixing in the rift valley of the Mid-Atlantic Ridge, *J. Phys. Oceanog., 32*, 1763–1778, 2002.

Urabe, T., E. T. Baker, J. Ishibashi, R. A. Feely, K. Marumo, G. J. Massoth, A. Maruyama, K. Shitashima, K. Okamura, J. E. Lupton, A. Sonada, T. Yamazaki, M. Aoki, J. Gendron, R. Green, Y. Kaiho, K. Kisimoto, G. Lebon, T. Matsumoto, K. Nakamura, A. Nishizawa, O. Okano, G. Paradis, K. Roe, T. Shibata, D. Tennant, T. Vance, S. L. Walker, T. Yabuki, and N. Ytow, The effect of magmatic activity on hydrothermal venting along the superfast-spreading East Pacific Rise, *Science, 269*, 1092–1095, 1995.

Von Damm, K. L., M. K. Brockington, A. M. Bray, K. M. O'Grady, and SouEPR Science Party, SouEOR 98: Extraordinary phase separation and segregation in vent fluids from the Southern East Pacific Rise, *Eos Trans. AGU, 80*(46), Fall Meet. Suppl., F1098–F1099, 1999.

White, R. S., D. McKenzie, and R. K. O'Nions, Oceanic crustal thickness from seismic measurements and rare earth element inversions, *J. Geophys. Res., 97*, 19,683–19,715, 1992.

White, R. S., T. A. Minshull, M. J. Bickle, and C. J. Robinson, Melt generation at very slow-spreading oceanic ridges: Constraints from geochemical and geophysical data, *J. Petrology, 42*, 1171–1196, 2001.

Wright, D. J., R. M. Haymon, S. M. White, and K. Macdonald, Crustal fissuring on the crest of the southern East Pacific Rise at 17°15′–40′S, *J. Geophys. Res., 107*, doi:10.1029/2001JB000544, 2002.

Figures and Captions:

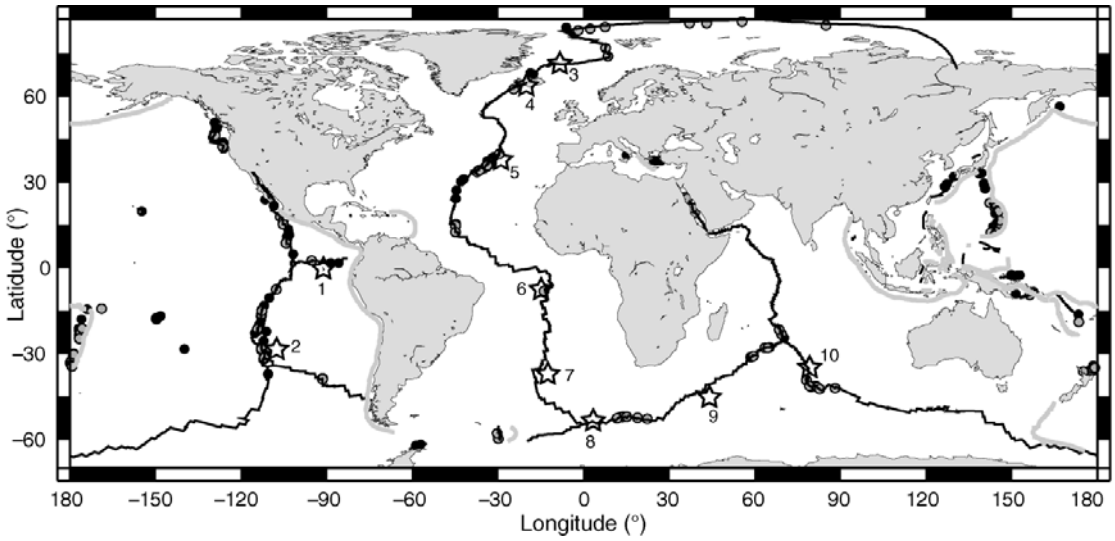

Figure 1a. Distribution of 144 known (black dots) and 133 inferred (gray dots) hydrothermal fields. Some individual fields contain several closely spaced (~100 m) "sites" distinctly named in the literature. Solid black lines are the midocean ridge and transform faults, gray lines are subduction zones. Hotspots (open stars) on or near (<500 km) the midocean ridge include 1, Galápagos; 2, Easter; 3, Jan Mayen; 4, Iceland; 5, Azores; 6, Ascension; 7, Tristan de Cunha; 8, Bouvet; 9, Crozet; and 10, Amsterdam-St. Paul.

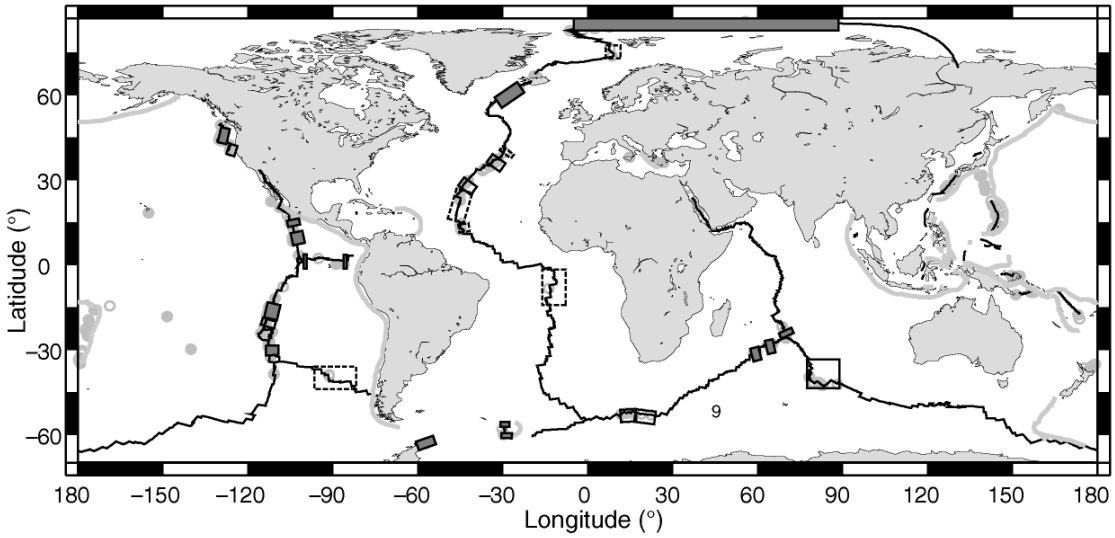

Figure 1b. Vent site distribution overlain with boxes indicating the quality of existing survey data along oceanic spreading ridges: densely surveyed (solid boxes), moderately well surveyed (open boxes), or sparsely surveyed (dotted line boxes).

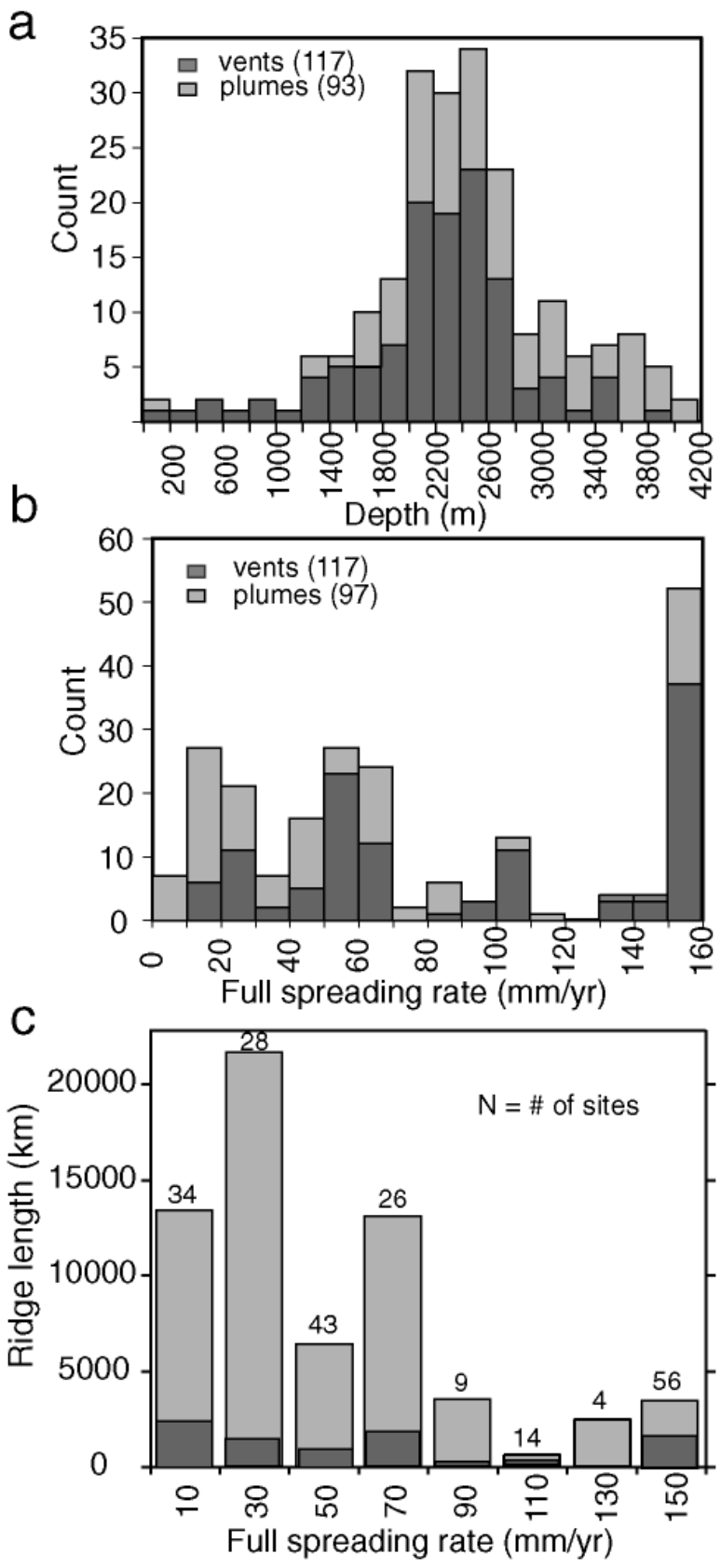
a
vents (117)
plumes (93)
Count
Depth (m)
b
vents (117)
plumes (97)
Count
Full spreading rate (mm/yr)
c
N = # of sites
Ridge length (km)
Full spreading rate (mm/yr)
34
28
43
26
9
14
4
56

Figure 2. (a) Frequency distribution of the depth of vent sites located along midocean ridge and back-arc basin spreading centers. (b) Frequency distribution of the full spreading rate at the vent site locations. (c) Frequency distribution for the full spreading rate of the global spreading center system in 20 mm/yr increments [*DeMets et al.*, 1990; *Bird*, 2003]. Numbers above each bar indicate the number of vent+plume sites in each spreading rate category. Dark bars at the bottom of each column indicate the approximate length of densely surveyed plus moderately surveyed ridge axis (from Figure 1b) in each spreading rate bin. This total includes more ridge sections than used in Table 1.

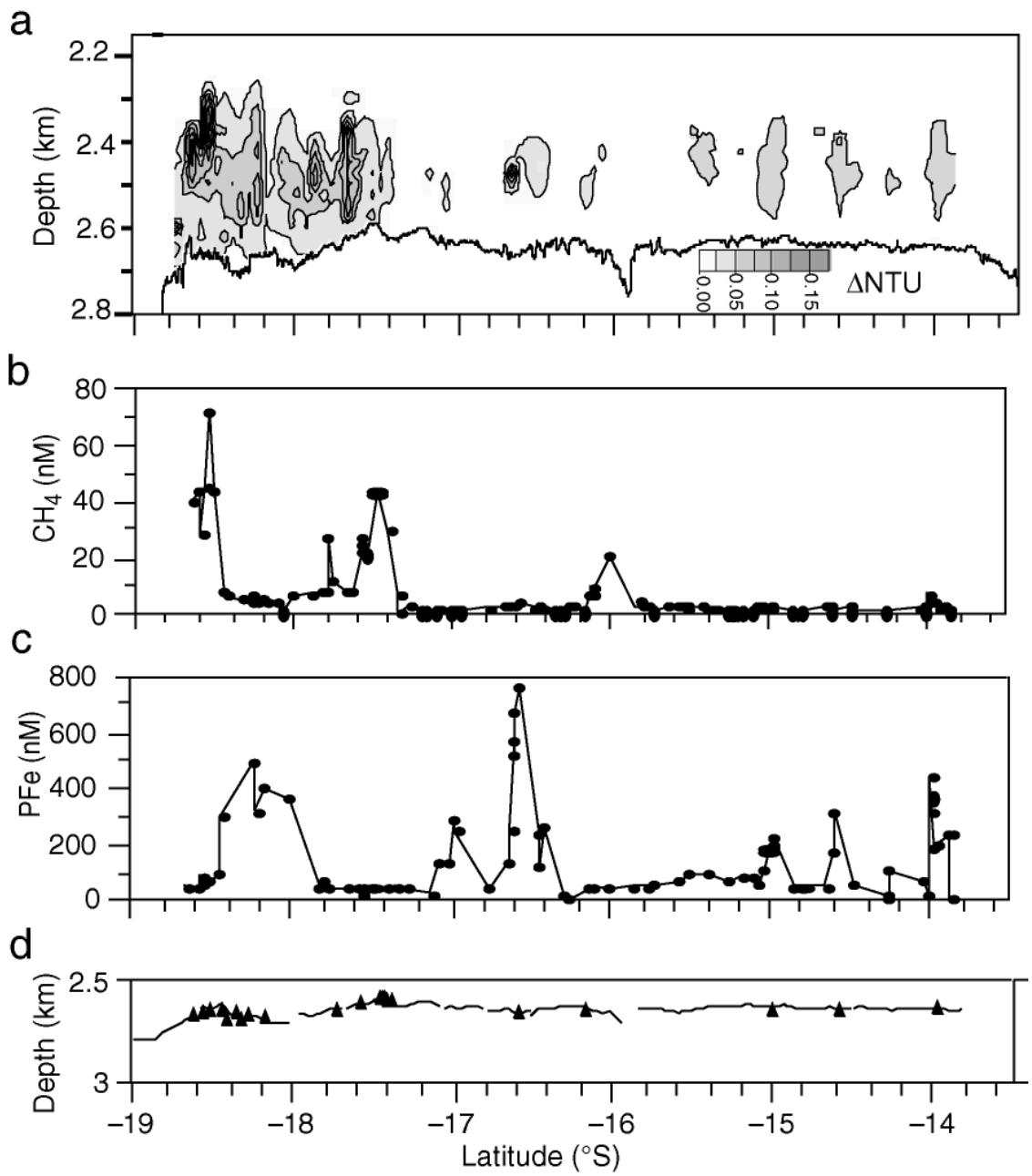

Figure 3. Along-axis transect of (a) light-scattering, (b) dissolved CH_4, and (c) particulate Fe from 13.5° to 18.67°S on the East Pacific Rise. Light-scattering data collected with a series of continuous CTDO tow-yos. Discrete CH_4 and Fe samples (solid circles) from bottle samples and vertical casts. Note that some plumes are volatile rich (e.g., near

18.5°S and 17.67°), while others are metal rich (e.g., near 18°, 16.5°, and 14°S). Location of known vent areas (solid triangles) shown in (d).

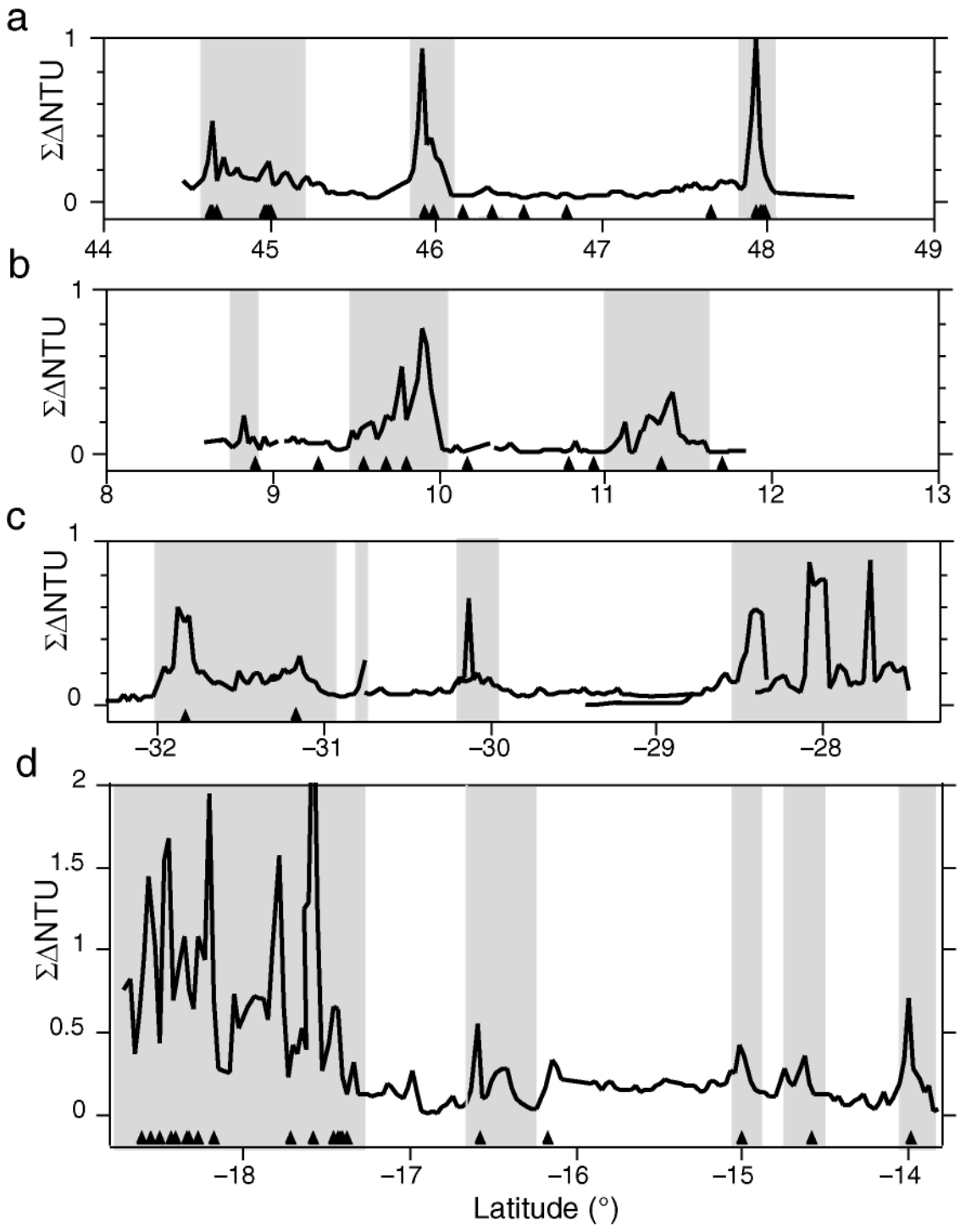

Figure 4. Vertically integrated ΔNTU transects from sections of fast ridges. ΣΔNTU values were determined by gridding continuous ΔNTU data into cells of 0.03° latitude along axis by 25 m thick from the top of the plume to the seafloor, then summing ΔNTU

values vertically in each latitude bin. Shaded areas identify regions where light-scattering plumes are continuous along axis. The fraction of the total surveyed areas covered by these regions (p_h) increases with increasing spreading rate: (a) Juan de Fuca Ridge (55 mm/yr), p_h = 0.23; (b) northern East Pacific Rise (103 mm/yr), p_h = 0.38; (c) southern EPR (148 mm/yr), p_h = 0.60; (d) southern EPR (148 mm/yr), p_h = 0.54. Locations of known vent fields (solid triangles) indicated along the bottom of each transect.

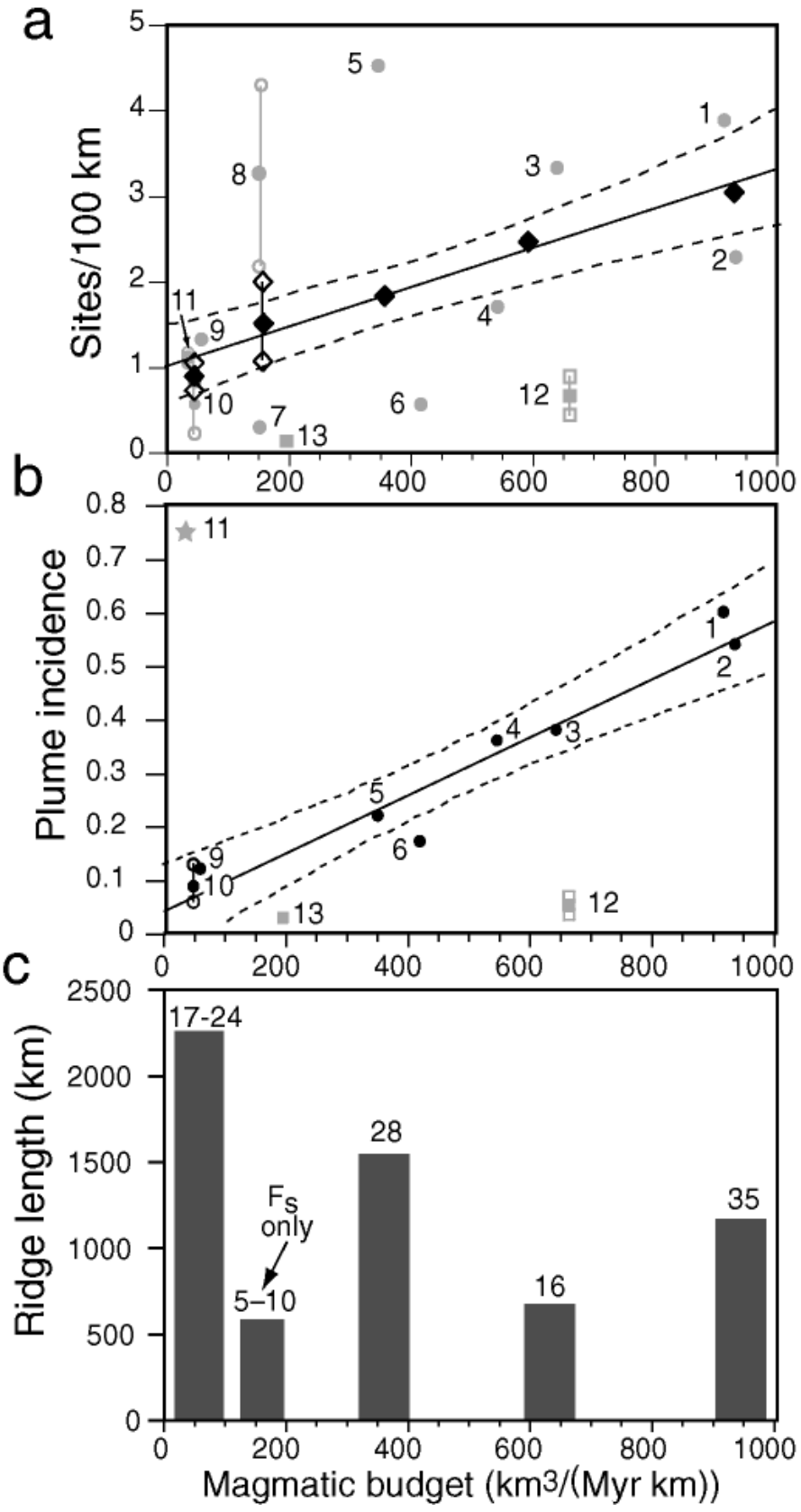
a
Sites/100 km
b
Plume incidence
c
Ridge length (km)
17-24
28
16
35
5–10
Fs only
Magmatic budget (km3/(Myr km))

Figure 5. (a) Scatter plot of hydrothermal sites/100 km of ridge length (F_s) vs. magmatic budget (V_m). Numbers refer to ridge sections identified in Table 1. Sections 8, 10, 11, and 12 show high and low estimates with open symbols, mean estimate with solid symbol. Squares indicate hotspot-affected ridges. Black diamonds show binned data (not including sections 12 or 13), with least-squares regression fit of $F_s = 1.01 + 0.0023V_m$ ($r^2 = 0.97$). 95% confidence bands for prediction of F_s from V_m given by dotted lines. (b) Plume incidence (p_h) vs. V_m, with symbols as in (a). Least-squares regression fit of $p_h = 0.043 + 0.00055V_m$ ($r^2 = 0.93$), excluding sections 11–13 (see text). Note also there is no data point for slow-spreading (non-hotspot-affected) ridges. (c) Total ridge length and number of vent sites in each of the five bins in (a).

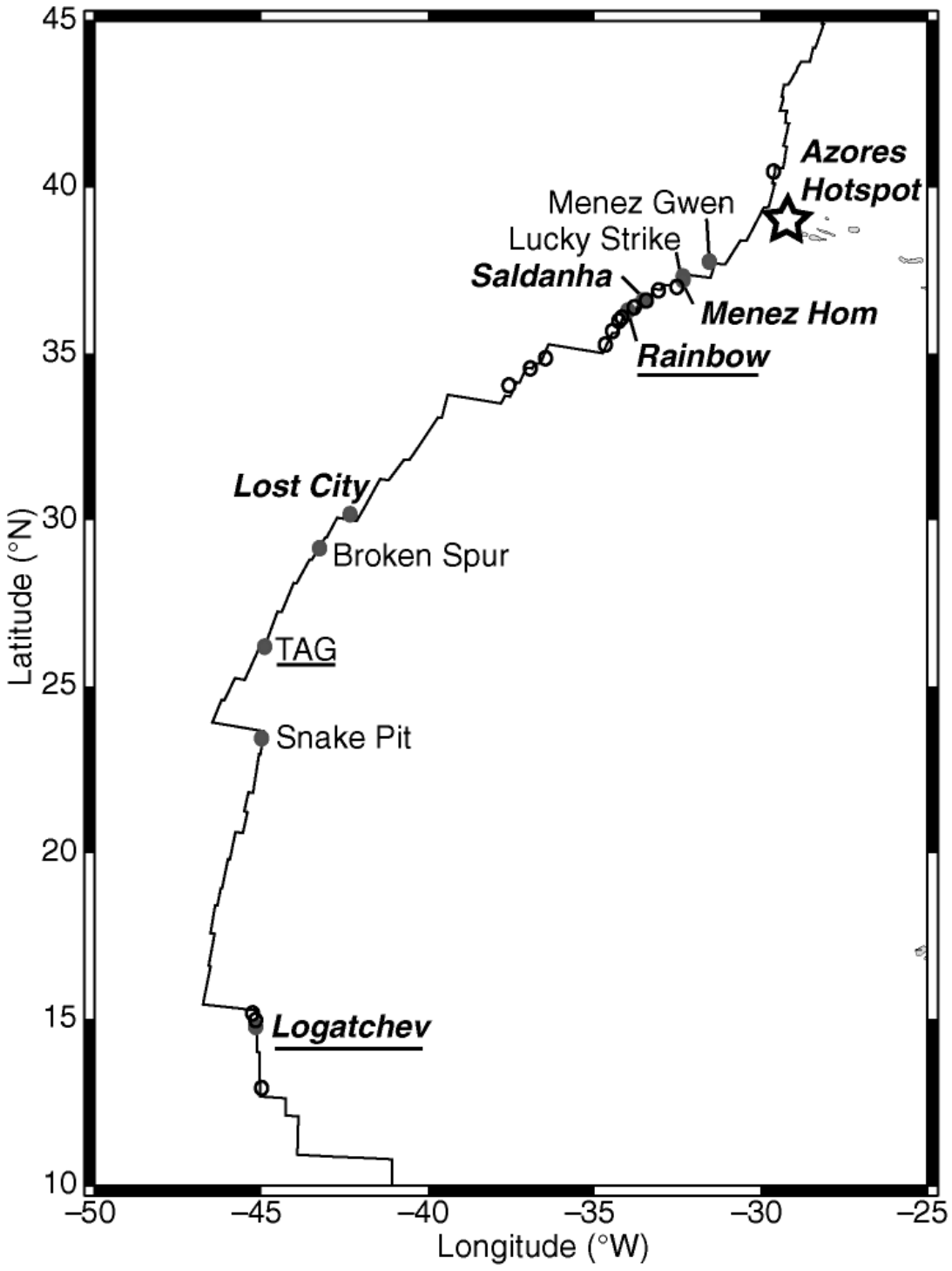

Figure 6. Known (solid circles) and inferred (open circles) vents sites along the northern Mid-Atlantic Ridge. Sites sited on axial neovolcanic highs are in plain type, sites hosted at least partially in ultramafic rocks are in italics, and sites apparently controlled by cross-

cutting fault populations are underlined. Unlike the situation on most fast-spreading ridges, many of the inferred vent sites are based on single vertical profiles and have a high degree of uncertainty.

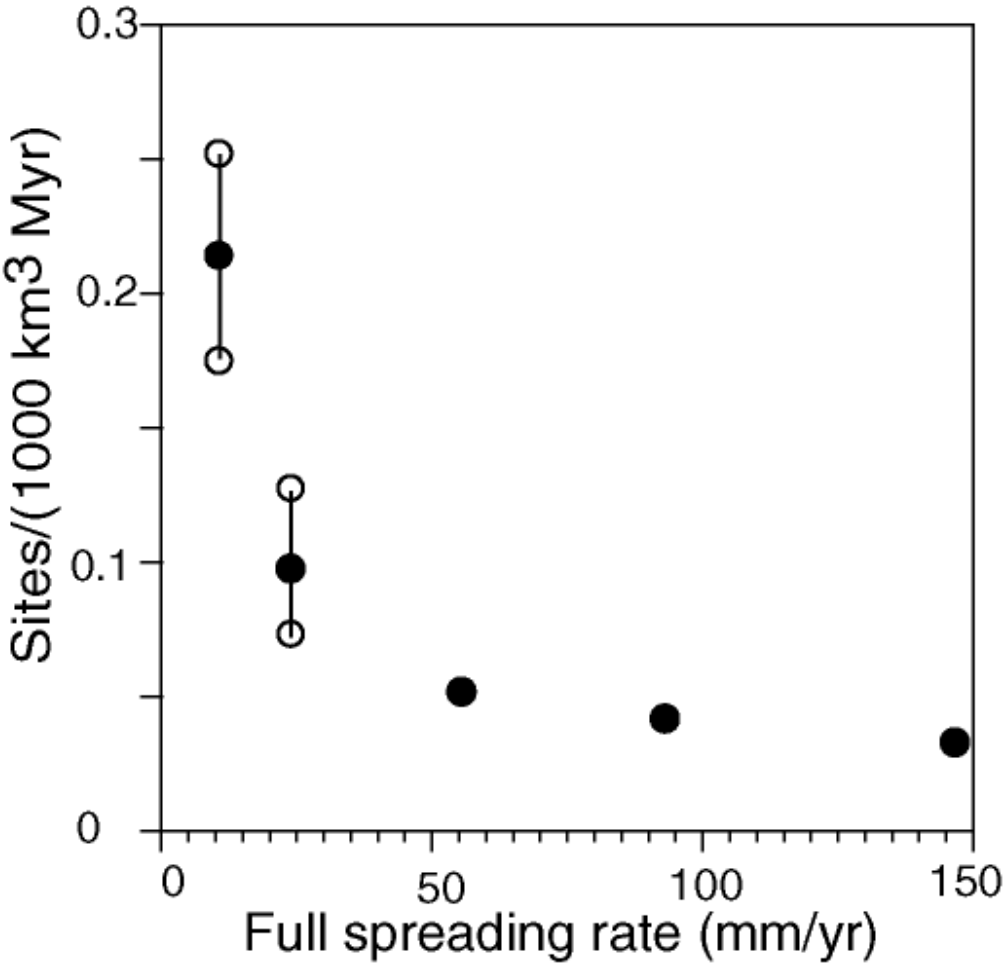

Figure 7. Site frequency Fs normalized to the magma delivery rate vs. spreading rate for the binned data in Figure 5a. Solid circles indicate mean values, open circles the uncertainty range (see Figure 5a). Approximately same trend would result using the ph data in Figure 5b (excluding the biased Gakkel Ridge result and the hotspot-affected ridge sections).

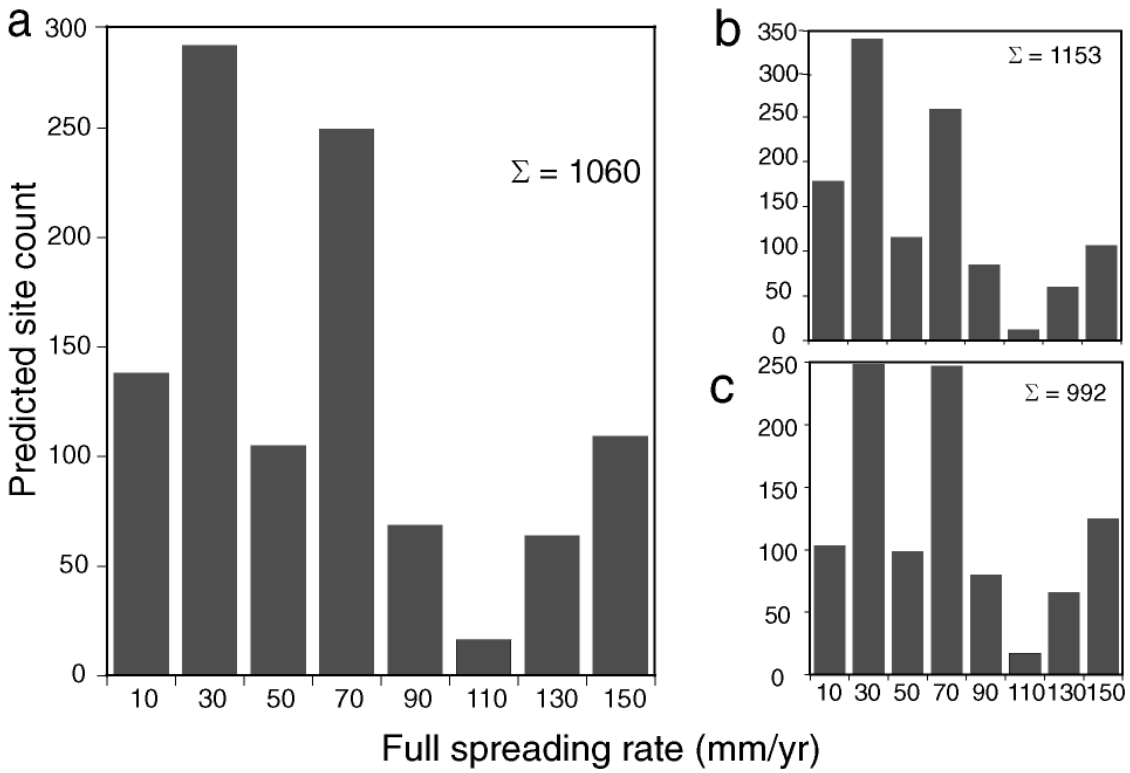

Figure 8. (a) Histogram of predicted vent site population as a function of spreading rate in 20 mm/yr bins (e.g., 0–20, 20–40, etc.). Total population on ridges is estimated as 1060. (b) and (c) show 95% confidence limits for high and low estimates, respectively.

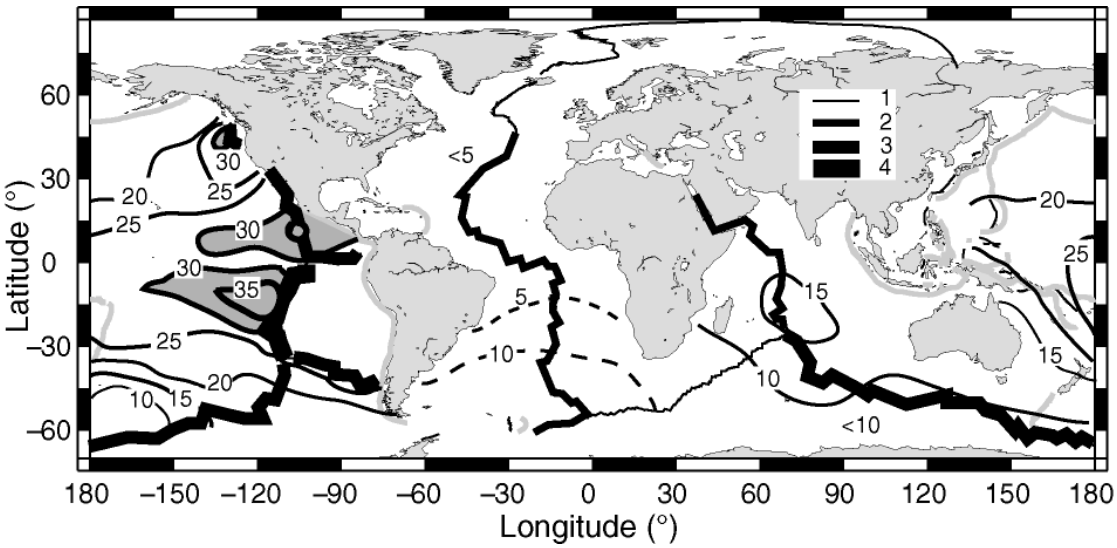

Figure 9. Deep-water (~2000–3000 m) distribution of δ(^{3}He)% values [*Geosecs Atlantic, Pacific, and Indian Ocean Expeditions*, 1987; *Lupton*, 1995, 1998; *Jamous et al.*, 1992; *Rüth et al.*, 2000] compared to ridge full spreading rates (δ(^{3}He)% = 100(R/R_{air} – 1); R = ^{3}He/^{4}He). Areas with δ(^{3}He)% values >30 are shaded. The MOR is divided into four rate categories corresponding to increasing line thickness: 1, <20 mm/yr; 2, 20–<50 mm/yr; 3, 50–100 mm/yr; 4, >100 mm/yr.

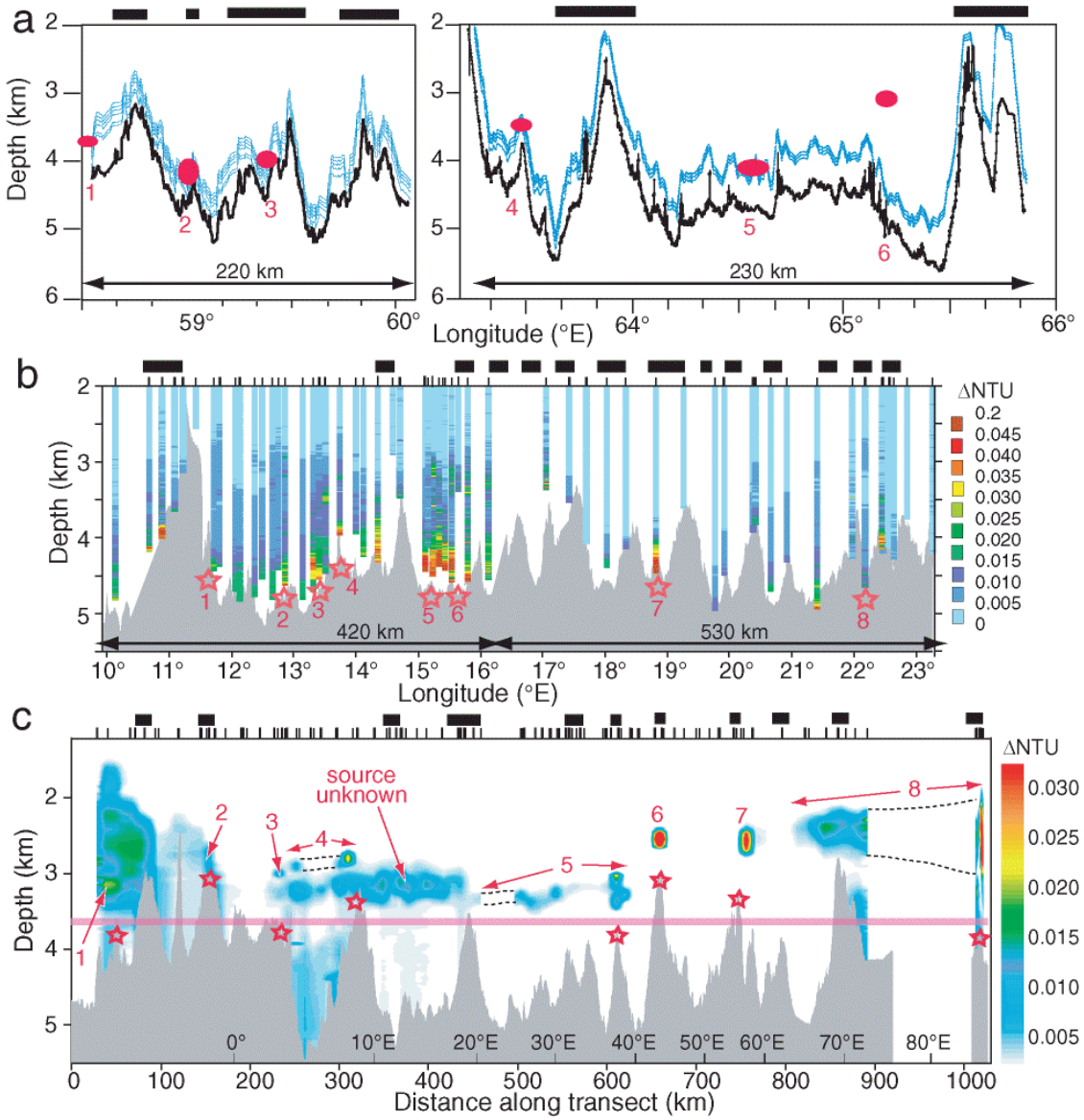

Plate 1. Along-axis transects of ΔNTU for the (a) SWIR 58.5°–66°E, (b) SWIR 10°–23°E, and (c) Gakkel Ridge (4°W–86°E). Black bars above each panel show approximate location of volcanic centers [*Grindlay et al.*, 1998; *Sauter et al.*, 2002; *Cannat et al.*, 2003; *Dick et al.*, 2003; *Michael et al.*, 2003]. In (a) the MAPR paths (light blue) intersected six incidences of ΔNTU (red symbols) while following the bathymetry (heavy black line).This diagram shows only one of two parallel tracks; the plume at 65.12°E was detected on the other track, which followed a slightly different bathymetry. In (b) ΔNTU data are displayed as individual profiles to avoid contouring artifacts. Not all casts were made at the rift axis, so profile depths may be deeper or shallower than the bathymetric

profile at the same longitude. Stars mark sites where hydrothermal activity is probable. In (c) MAPR data was sufficiently dense to contour [*Baker et al.*, 2004]. Numbers mark individual plumes and the possible seafloor source location of each is shown by the underlying stars; source location of the extensive plume from 250–450 km along section, centered at ~3200 m, is unknown. Most of the ΔNTU anomaly west of ~150 km has no thermal expression and is thus nonhydrothermal [*Baker et al.*, 2004]. Supplementary x-axis scale gives longitude along the transect. Pink line indicates approximate top of the bottom isopycnal layer.

Table 1. Determinations of Site Frequency, Plume Incidence, and Magmatic Budget for Selected Ridge Sections

Location	ID #	km	# of active sites[a]	F_s sites/ 100 km	p_h: transect[b]	p_h: % of profiles[c]	Avg. full spreading rate (mm/yr)[d]	Crustal thick-ness (km)[e]	Magmatic budget (km^3/(Myr km))	Refs.[f]
"Fast" Ridges										
EPR 14°–19°S	1	540	21	3.89	0.60		145.0	6.3	914	1
EPR 27°–32°S	2	610	14	2.30	0.54		148.0	6.3	932	2
EPR 9°–13°N	3	300	10	3.33	0.38		101.4	6.3	639	3
EPR 15°–18°N	4	350	6	1.71	0.36		86.0	6.3	542	4
JDFR+Explorer	5	480	22	4.53	0.21		55.0	6.3	347	5
SEIR normal	6	1050	6	0.57		0.17	66.0	6.3	416	6
"Slow" Ridges										
MAR 27°–30°N	7	330	1	0.30			24.0	6.3	151	7
MAR 36°–38°N (min)		230	5	2.17			23.9	6.3	151	8
MAR 36°–38°N (max)		230	10	4.35			23.9	6.3	151	8
MAR 36°–38°N (avg)	8	230	7.5	3.26			23.9	6.3	151	8
SWIR 58°–66°E	9	450	6	1.33	0.12		14.0	4	56	9
SWIR 10°–24°E (min)		950	2	0.21		0.058	11.2	4	45	10
SWIR 10°–24°E (max)		950	8	0.84		0.13	11.2	4	45	10
SWIR 10°–24°E (avg)	10	950	5	0.53		0.087	11.2	4	45	10
Gakkel R. (min)		850	9	1.06	0.75		8.5	4	34	11
Gakkel R. (max)		850	10	1.18	0.75		8.5	4	34	11
Gakkel R. (avg)	11	850	9.5	1.12	0.75		8.5	4	34	11
Hotspot Ridges										
Reykjanes R.	12	750	1	0.13	0.012		19.1	10	191	12
SEIR Hotspot (min)		445	2	0.45		0.034	66.0	10	660	6
SEIR Hotspot (max)		445	4	0.90		0.069	66.0	10	660	6
SEIR Hotspot (avg)	13	445	3	0.67		0.052	66.0	10	660	6

[a] Site listings available at http://www.interridge.org

[b] p_h calculated from contoured plume data.

[c] p_h calculated from percent of profiles detecting a plume.

[d] *DeMets et al.* [1990].

[e] Average crustal thickness for "normal" ridge (6.3 km), ultraslow-spreading ridges (4 km), and hotspot-affected ridges (10 km) [*White et al.*, 1992, 2001].

[f] (1) *Baker and Urabe* [1996]; (2) *Baker et al.* [2002]; (3) *Baker et al.* [1994]; (4) *Baker et al.* [2001b]; (5) *Baker and Hammond* [1992], E.T. Baker, unpublished data; (6) *Scheirer et al.* [1998]; (7) *Murton et al.* [1994]; (8) *Langmuir et al.* [1993], *Fouquet et al.* [1995], *German et al.* [1996a], *Barriga et al.* [1998], *Fouquet et al.* [2002]; (9) *German et al.* [1998a]; (10) *Bach et al.* [2002], *Baker et al.*, in press; (11) *Edmonds et al.* [2003], *Baker et al.*, in press; (12) *German et al.* [1994]. Additional references available at http://www.interridge.org.

Table 1. Determination of Site Frequency, Plume Incidence, and Magmatic Budget for Selected Ridge Sections